FINAL PUBLISHABLE REPORT

Grant Agreement number	15SIB01
Project short name	FreeFORM
Project full title	Reference algorithms and metrology on aspherical and freeform lenses

Project start date and duration:	June 2016, 36 months	
Coordinator: Dr. -habil. Hichem Nouira, LNE	Tel: +33 140 433 763	E-mail: hichem.nouira@lne.fr
Project website address: http://www.ptb.de/empir/freeform-home.html		
Internal Funded Partners: 1- LNE, France 2- CMI, Czech Republic 3- PTB, Germany 4- SMD, Belgium 5- TUBITAK, Turkey 6- VTT, Finland	External Funded Partners: 7- ENS-Cachan, France 8- IPP, Czech Republic 9- UEF, Finland 10- UNOTT, United Kingdom 11- USTUTT, Germany	Unfunded Partners: 12- AIST, Japan 13- FU, China 14- GEOMNIA, France 15- IBSPE, The Netherlands 16- POLYU, Hong Kong 17- Thales Agx, France 18- TRIOPTICS, Germany 19- UnB, Brazil
RMGs: -		

This publication reflects only the author's view and the Commission is not responsible for any use that may be made of the information it contains.

The EMPIR initiative is co-funded by the European Union's Horizon 2020 research and innovation programme and the EMPIR Participating States

TABLE OF CONTENTS

1 Overview

Aspheric and freeform surfaces are a class of optical elements with diverse and growing applications in photonics. Their use has grown considerably in the last few years because aspheres and freeform surfaces are superior to classical spherical optics but form metrology is a limiting factor. Thus, there was an urgent need to strengthen and harmonise the metrology for optical surfaces.This project focused on the development of i) reference algorithms to analyse form, ii) reference standards and iii) improved facilities for aspherical and freeform optical elements traceable to the SI metre definition with an uncertainty below 30 nm. The outcomes of this project will result in progress in the photonics research and industry sectors.

2 Need

In Europe, the photonics industry employs more than 2 million people and this is expected to double by 2020. Aspheres and freeform surfaces have diverse and growing applications in imaging systems (e.g. medical, safety, automotive, energy and defence applications), astronomy, lithography and synchrotron techniques. Due to their degrees of freedom, optical systems that use aspheres (e.g. cameras, satellites, medical devices, vision systems, smartphones and synchrotrons) tend to have fewer optical elements, which means lower production costs and weight, and higher imaging quality.

Within the EMRP project IND10, an uncertainty below 100 nm was achieved for aspheres and, in some selected samples, an uncertainty of 50 nm could even be obtained. Nevertheless, for high quality optical surfaces metrology, optics manufacturers and manufacturers of optics metrology instruments or polishing machines required improved metrological capabilities and high-accuracy traceability chains at NMIs/DIs. To guarantee this for asphere and freeform, it was necessary to develop reference least squares (L_2) and Min-Max (L_∞) algorithms enabling the robust analysis of measurements data and to develop suitable reference optical standards made of thermo-invariant materials.

Form metrology for optical aspheres and freeforms below 30 nm uncertainty level was considered a critical need for research institutes and industry. This need to develop accurate form metrology for asphere and freeform optics was strongly emphasised during ongoing discussions conducted at the High Level Expert Meetings and workshops of the Competence Centre for Ultra-Precise Surface Manufacturing (CC UPOB).

3 Objectives

The overall objective of this project was to build a traceability chain with an uncertainty below the 30 nm level. The specific objectives of this project were to:

1. **Develop robust reference least-squares (L_2) and Min-Max (L_∞) minimisation algorithms** including the generation of reference data (softgauges) and recommendation on the reference mathematical model for aspheres and freeforms optical elements. The algorithms will allow asphere and freeform evaluation to sub-nanometre accuracy.
2. **Develop advanced techniques for data analysis** (alignment/registration techniques, stitching algorithms, data fusion, interpolation methods and improved filtering methods) to support the experiments. To apply the algorithms to measurement datasets provided by the partners. To estimate the uncertainty of the reconstruction results with respect to the Guide to the Expression of Uncertainty in Measurement (GUM) and apply it for the determination of the uncertainty of measurement for the calibration of aspheres and freeform lenses.
3. **Design, manufacture and characterise innovative aspherical and freeform optical reference elements**, made of thermo-invariant materials to develop a reference calibration chain at European NMIs, and to facilitate the transfer of traceability between NMIs, standardisation organizations, research laboratories and end users. The target uncertainty for the radius measurements of the thermo-invariant asphere and freeform materials is less than 100 nm.
4. **Improve measurement capabilities of NMIs and DIs on aspherical and freeform standards** for high-level areal and single point scanning reference measurement systems, achieving an uncertainty of less than 30 nm. This will involve the improvement of reference metrology instruments ensuring

tactile and/or optical measurements such as ultra-high precision single point and optical imaging instruments.

5. **Develop a strategy for the long-term operation of the capability developed** including the take up of the technology and measurement infrastructure developed by the project. Two case studies on the application of the developed reference fitting algorithms and on the improvement of the metrology chain for innovative 3D printed precision freeform optics will be performed.

4 Results

This project investigated three main elements of the metrology chain for optical surfaces with complex shape (asphere and freeform), as shown in Figure 1. The project focused on the development of reference algorithms, reference thermo-invariant standards and reference metrology for aspherical and freeform optical elements traceable to the SI meter definition with the aim of building a traceability chain with an uncertainty below the 30 nm level.

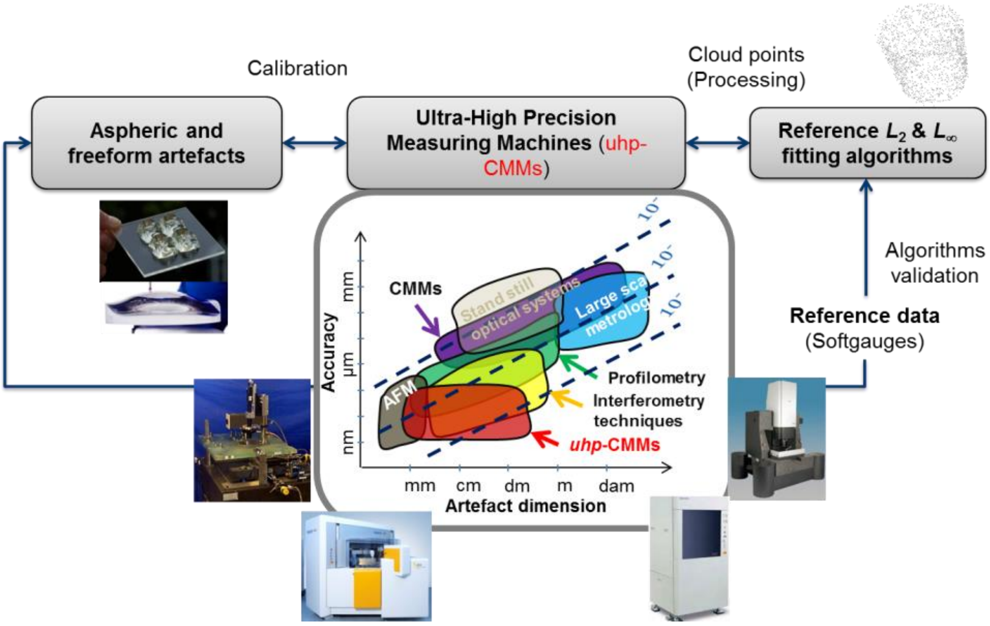

Figure 1: Description of the whole metrology chain for form error metrology (case of aspheres and freeforms)

Objective 1: Develop robust reference least-squares (L_2) and Min-Max (L_∞) minimisation algorithms

Ultra-high precision measuring machines enable to measure aspheric shapes with an uncertainty of few tens of nanometres. The resulting clouds of points are then associated to theoretical model at the same level of accuracy so as to obtain parameters that indicate about form error. Minimum zone (MZ), defined as the least value of peak to valley (PV), is widely used to assess form error. Least squares method (L_2) is often used to determine MZ but the resulting value is usually overestimated. For this reason, L_2 is replaced by L_∞ norm because it gives a more accurate value of MZ since it directly minimizes PV. Using L_∞ norm results in a non-smooth optimization problem and consequently its resolution becomes more challenging compared to L_2.
In this project, a novel minimax fitting method for accurate metrology of aspheres and freeform based on a hybrid trust region algorithm (HTR) was proposed. To assess performance of the introduced method, it was compared to an available minimax fitting algorithm based on a smoothing technique: exponential penalty function (EPF). The choice of EPF is justified by superior performances in comparison to existing techniques. Comparison was conducted on reference data, data available in literature and data gathered form measurements of a real optical high quality asphere.

<u>**Hybrid Trust Region algorithm (HTR**</u>)

The HTR algorithm enables to perform trust region step, line search step or curve search step according to the specific situation faced at each iteration. It avoids solving the trust region problem many times.
For every iteration, a trust region trial step d_k was obtained by solving the quadratic problem given in (1).

$$QP(x_k, B_k):\begin{cases} \min_{(d,z)\in R^{n+1}} \frac{1}{2} < d, B_k d > +z = M_k(d,z), \\ \text{s.t.} \quad < \nabla f_i(x_k), d > -z \le \phi(x_k) - f_i(x_k), \quad i = 1, \dots, m \\ \|d\|_\infty \le \Delta_k \end{cases} \tag{1}$$

Where $\boldsymbol{B_k}$ is *n* by *n* symmetric positive definite matrix, Δ_k is the parameter defining the trust region domain, z is an introduced parameter depending on the first derivative of the objective function ϕ, ∇f_i is the gradient of the function f_i and " $<.,.>$ " denotes the dot product.

The trust region domain was defined using L_∞ instead of L_2 so as QP becomes an easily-solved quadratic problem. It should be mentioned that the proposed QP in (1) has always a solution since $(0,0)$ lies inside the feasible domain. This problem could be solved using classical methods adapted to quadratic problems such as interior point method

If the resulting trust region trial step d_k could not be accepted, a corrected step $d_k + \tilde{d}_k$ was determined by solving the problem in (2).

$$\widetilde{QP}(x_k, B_k):\begin{cases} \min_{(\tilde{d},z)\in R^{n+1}} \frac{1}{2} < d_k + \tilde{d}, B_k(d_k + \tilde{d}) > +\tilde{z} = \widetilde{M}_k(\tilde{d},\tilde{z}), \\ \text{s.t.} \quad < \nabla f_i(x_k), \tilde{d} > -\tilde{z} \le \phi(x_k + d_k) - f_i(x_k + d_k), \quad i = 1, \dots, m \\ \left\|d_k + \tilde{d}\right\|_\infty \le \Delta_k \end{cases} \tag{2}$$

If neither the initial trust region step d_k nor the corrected step $d_k + \tilde{d}_k$ could be acceptable in the trust region scheme, a line search along d_k or a curve search was performed if d_k is a descent direction (the actual reduction $r_k > 0$ in (4)). Otherwise ($r_k \le 0$), a curve search is used to find a step length t_k that verifies (3).

$$\phi\left(x_k + t_k d_k + t_k^2 \tilde{d}_k\right) \le \phi(x_k) - \alpha t_k < d_k, \boldsymbol{B_k} d_k > \tag{3}$$

Where $\alpha \in (0, 1/2)$, d_k is the solution of (1) and $\tilde{d}_k$ is the solution of (2). In the case $\|d_k\| \le \|\tilde{d}_k\|$, $\tilde{d}_k$ should be taken to be 0. The implemented algorithm follows the next steps:

- Step 1: Give initial values $x_0 \in R^n, \varepsilon > 0, \Delta_{max}, \Delta_0 \in (0, \Delta_{max}), 0 < \tau_1 < 1 < \tau_2, \alpha \in (0,1/2)$, $\beta \in (0,1/2)$, $0 < \mu < 2\alpha$, $\eta \in (0.5, 1)$, $\boldsymbol{B_0} = \boldsymbol{I}$, $k := 0$.
- Step 2: Determine (d_k,z_k) by solving the quadratic problem. If $\|d_k\| \le \varepsilon$, stop; Otherwise;
- Step 3: Compute the ratio between the actual reduction and the predicted reduction

$$r_k = \frac{\phi(x_k) - \phi(x_k + d_k)}{M_k(0,0) - M_k(d_k, z_k)} \tag{4}$$

- Step 4: (Update the iteration point)
  (4.1) If $r_k > \mu$, set $s_k = d_k$, $x_{k+1} = x_k + s_k$, go to step 5; Otherwise;
  (4.2) Compute the second-order correction step $\tilde{d}_k$ by solving problem (2), In the case $\|d_k\| \le \|\tilde{d}_k\|$, $\tilde{d}_k$is set to be 0.
  (4.3) Compute corrected $\tilde{r}_k$

$$\tilde{r}_k = \frac{\phi(x_k) - \phi\left(x_k + d_k + \tilde{d}_k\right)}{M_k(0,0) - M_k(d_k, z_k)} \tag{5}$$

  (4.4) If $\tilde{r}_k > \mu$, set $r_k = \tilde{r}_k$, $s_k = d_k + \tilde{d}_k$, $x_{k+1} = x_k + s_k$, go to step 5; Otherwise
  (4.5) If $r_k > 0$, set $\tilde{d}_k = 0$
  (4.6) (Perform curve search) Compute t_k: the first number in the sequence of $\{1, \beta, \beta^2, \dots\}$ to verify (3). Set $s_k = t_k d_k + t_k^2 \tilde{d}_k$ and $x_{k+1} = x_k + s_k$.
- Step 5: (Update Δ_k)
  If $r_k \le \mu$, $\Delta_{k+1} \in [\|s_k\|, \tau_1 \Delta_k]$
  If $r_k \ge \eta$, $\Delta_{k+1} = min(\tau_2 \Delta_k, \Delta_{max})$
  Otherwise, $\Delta_{k+1} = \Delta_k$
- Step 6: (Update $\boldsymbol{B_k}$), Update $\boldsymbol{B_k}$ to $\boldsymbol{B_{k+1}}$; $k := k + 1$, go to step 1

To update $\mathbf{B_k}$, the Powell's modification of BFGS formula was used. The principle of the trust region method is shown in figure 2.

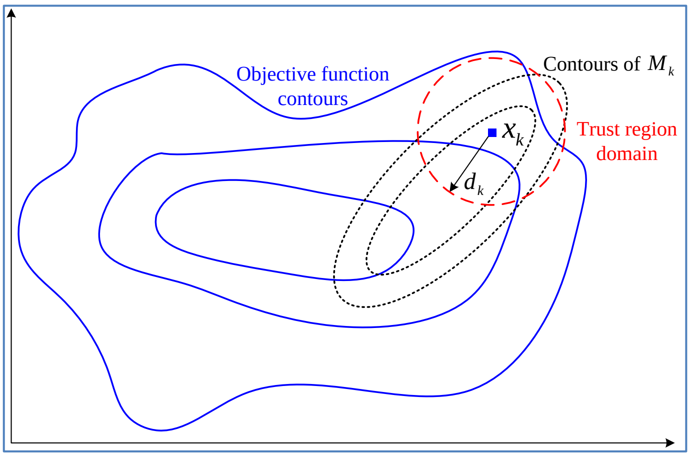

Figure 2: Illustration of Trust Region method

Numerical validation

a. Requirements of reference data

For the evaluation, reference data are inputted to the software under test, the returned value is compared to the reference measurand and then a decision could be made whether the software is accepted or rejected. Reference data should satisfy input requirements specified in the description of the algorithm under test and this may include:

Data extraction: For some CMMs using tactile probes, recorded data has a constant sampling step along X and Y directions. The included software needed the value of the sampling step to perform calculations. The considered reference data must also follow this specification and a set of data with a varying sampling step must not be taken as a reference data for this software.
Uniqueness of the solution: Reference data must have a unique associated reference measurand value. This problem was outlined by Shakarji *et.al* in for the problem of maximum inscribed circle determination.
Number of points: The number of points contained in the reference data set was taken according to the software specifications. Some algorithms were only applied if the number of recorded points was not high.
Uncertainty: Uncertainty of the reference value of the measurand must also be given in order to make comparisons to the results obtained by the software under test. The associated uncertainty to the reference data is purely numerical. It is based on uncertainties of the different steps of the generation algorithm. The final uncertainty could be calculated by the mean of uncertainty propagation rules when the generation algorithm is relatively simple. Monte Carlo simulations could also be used in other cases.
Stability: Designed reference data must be stable. In fact, a small perturbation in the designed data must not affect the reference value of the measurand too much.
Vertex, non-vertex solution: Generating reference data for Chebyshev fitting is based on formulating optimality conditions of the problem. For the formal case, the solution lies in the vertex of the feasible domain. Some algorithms might be designed to target vertices of feasible domain to rapidly converge to the solution. Hence, they could not find non-vertex solutions. Designed reference data must be aligned with this requirement and give either a vertex or non-vertex solution according to the algorithm specification.
Deviation error value: In some cases, fitting algorithms could not be used if the value of form error exceeds a given value. Generally, this is expressed as a percentage of a characteristic dimension of the artefact. In least squares fitting for instance, calculation of the Hessian matrix is based on neglecting second order derivatives of residuals. For the case where the deviation values become high, this approximation is no longer valid and the resulting Hessian matrix is not accurate. Therefore, the returned results are not exact.
Initial alignment value: Initial position of measured data relatively to reference shape highly affects performances of fitting algorithms. Most fitting software underlies inner routines to perform a rough

alignment to make measured data as close as possible to reference model. Some algorithms could only perform fitting if the input data points are well aligned with the model. Calculation of foot points which is a crucial step in approximately all fitting algorithms is highly affected by the initial position of the input data.

Error-free: Validation of algorithms must be performed in the perfect operator approximation. In fact, when testing a given algorithm, the submitted data must be error-free. This means that measuring errors must not be embedded in designed data. Taking input data that include measuring errors make decision making difficult since we cannot tell whether inaccuracy results from measurement or processing.

A literature method suggested by A. Forbes for reference data generation was adapted to aspherical surfaces for the case of LS and MZ fitting. The main idea behind reference data generation is to state the optimality conditions for the considered fitting problem and then derive data sets that perfectly meet these conditions. For LS fitting, the method is called the null-space method since it is based on the determination of the null-space of the Jacobian matrix. For MZ fitting, Karush-Kuhn-Tucker (KKT) conditions are used for data generation.

b. Application on reference data

A set of reference datasets with previously known peak to valley (*PV)* value (PV_{ref}) were generated (Figure 3). The main idea was to state optimality conditions and then derive datasets for which optimality conditions are automatically met. It should be noted that in the case of aspheric shapes, this method could only generate vertex solutions. For the validation process, only transformation parameters were sought. Surface nominal coefficients were supposed known. Five configurations of coefficients were used (Table 1). These coefficients were chosen to provide different slope values to the nominal aspheric shape. For each configuration, data with predefined number of points (N=121, 1024, 10404 and 100489) and a previously known PV_{ref} ($PV_{ref}=10^{-4}$) were generated.

Table 1: Surface nominal coefficients used for reference data generation

Coefficients Configuration	R (*mm*)	κ	a_4 (*mm*$^{-3}$)	a_6 (*mm*$^{-5}$)	a_8 (*mm*$^{-7}$)	a_{10} (*mm*$^{-9}$)	R_{max} (*mm*)	Slope (°)
I	101.58	-1	-1.70 x10^{-13}	-8.51 x10^{-14}	-4.25 x10^{-14}	-2.12 x10^{-14}	20	5
II	19.79	-0.9	-1.51 x10^{-17}	-7.55 x10^{-18}	-3.77 x10^{-18}	-1.88 x10^{-19}	20	25
III	8.88	-0.8	-1.94 x10^{-12}	-9.72 x10^{-13}	-4.86 x10^{-13}	-2.43 x10^{-13}	20	45
IV	4.14	-0.9	-4.17 x10^{-12}	-2.08 x10^{-12}	-1.04 x10^{-12}	-5.21 x10^{-13}	20	65
V	0.77	-1	-2.22 x10^{-11}	-1.11 x10^{-11}	-5.56 x10^{-12}	-2.78 x10^{-12}	20	85

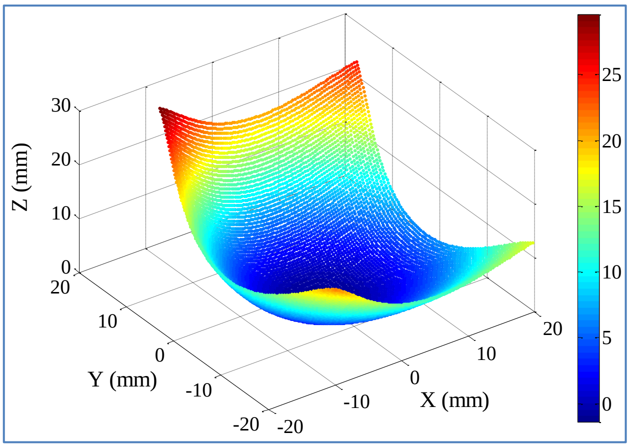

Figure 3: Generated reference dataset (10 404 points)

In order to assess the performance of the proposed algorithm in regard to the Exponential Penalty Function algorithm (EPF), each generated dataset was submitted at the same time to both algorithms: EPF and HTR. The corresponding *PV* values respectively PV_{EPF} and PV_{HTR}, as well as execution time, respectively T_{EPF} and T_{HTR}, were compared as described in figure 4. Initial data was rotated by angle $\pi/20$ around *x* axis and $\pi/15$ around *y* axis as well as translated by -1 *mm* in *x* direction, 1 *mm* in *y* direction and -1 *mm* in *z* direction.
Tables 2, 3 and 4 illustrate the obtained values of $PV\text{-}PV_{ref}$ as well as execution time for both algorithms. Concerning *PV* values, both algorithms provided enough accurate results, although HTR showed superior results for all test cases. In fact, for approximately all generated data points, HTR returned *PV* values ten times more accurate than EPF. HTR clearly overpowered EPF on execution time, with EPF execution time five times higher than the HTR, especially for data points that exceed 1 000 points.

Table 2: Values of $PV\text{-}PV_{ref}$ and execution time for HTR and EPF (configuration II)

N	$PV_{HTR}\text{-}PV_{ref}$ (mm)	$PV_{EPF}\text{-}PV_{ref}$ (mm)	T_{HTR} (s)	T_{EPF} (s)
121	4.06×10^{-19}	1.45×10^{-15}	0.84	2.68
1024	9.50×10^{-16}	1.11×10^{-16}	2.07	9.15
10404	1.78×10^{-16}	4.51×10^{-13}	12.1	61.91
100489	1.64×10^{-16}	4.92×10^{-15}	41.51	226.96

Table 3: Values of $PV\text{-}PV_{ref}$ and execution time for HTR and EPF (configuration III)

N	$PV_{HTR}\text{-}PV_{ref}$ (mm)	$PV_{EPF}\text{-}PV_{ref}$ (mm)	T_{HTR} (s)	T_{EPF} (s)
121	4.24×10^{-15}	1.13×10^{-14}	2.18	2.48
1024	2.18×10^{-16}	2.61×10^{-16}	4.32	4.47
10404	1.41×10^{-15}	3.08×10^{-15}	4.27	36.50
100489	6.73×10^{-15}	6.78×10^{-15}	20.52	255.06

EPF consists of approximating the non-differentiable objective function by a smooth one (differentiable function) at each iteration and then minimizes it. The Newton method was used so the hessian matrix was calculated. Since the hessian matrix calculation time is proportional to the number of points in the data set, the execution time increases even when considering an active set. Moreover, descent direction determination is not always accurate since the obtained hessian matrix is not positive definite all the time. Hence, corrections were brought to the hessian matrix whenever was needed.
On the other hand, when establishing the *QP* for HTR algorithm, the matrix $\boldsymbol{B}$ was chosen to be symmetric positive definite, and the Powell's modification of BFGS formula proved to be efficient for this purpose without the need to calculate second order derivation terms, which considerably reduces execution time.

Table 4: Values of $PV\text{-}PV_{ref}$ and execution time for HTR and EPF (configuration IV)

N	$PV_{HTR}\text{-}PV_{ref}$ (mm)	$PV_{EPF}\text{-}PV_{ref}$ (mm)	T_{HTR} (s)	T_{EPF} (s)
121	4.03×10^{-15}	9.78×10^{-14}	1.14	1.79
1024	8.14×10^{-16}	8.42×10^{-15}	5.23	7.24
10404	1.15×10^{-16}	2.14×10^{-15}	35.88	200.16
100489	9.86×10^{-15}	1.05×10^{-14}	50.03	274.75

c. Application on benchmark data

The proposed algorithm was tested using data already available in published literature. We refer to where a heuristic method based on differential evolution algorithm (DE) was developed and a data set of 8100 points were used to verify the algorithm. The nominal coefficients of the aspheric surface are: R=520, κ=-0.7, a_4=5.2 10^{-5}, a_6=-6.5 10^{-6}, a_8=3.11 10^{-8}, a_{10}=3.222 10^{-9}. Fractal Brownian function was used to generate noise with amplitude σ=1 µm around the nominal surface. The same data points were adopted for a comparison between EPF and DE in [6].

Table 5 illustrates a comparison of results obtained by EPF and HTR, *PV* value given by the formal algorithm was 3.2 µm. The newly proposed HTR algorithm provided a smaller value of 3.1 µm, which was approximately 60 nm lower. A 60 nm difference could cause an aspheric lens to be rejected while it is conforming to specifications. The two values were approximately similar regarding execution time.

d. Experimental investigation

A high quality optical aspherical lens, manufactured by Anteryon® company using a Single Point Diamond Turning (SPDT) process and finished with a high precision polishing process and glass coating, was selected for test. The intrinsic parameters of the AO775 asphere were:

- curvature at the apex is equal to $c = 10^{-20}$ mm^{-1},
- conic constant is $\kappa = -1$
- asphere coefficients are: $a_2 = 0.0223$, $a_4 = 7.293\ 10^{-6}$, $a_6 = 4.52\ 10^{-9}$, $a_8 = -1.061\ 10^{-11}$ and $a_{10} = 9.887\ 10^{-15}$
- sag $S = 3.217$ mm
- clear aperture $CA = 11.74$ mm.

The asphere was scanned with an ultra-high precision measuring machine, designed specifically for non-contact measurement of aspherical and freeform optics. The measurement uncertainty was mainly determined by the metrology loop between the probe and the artefact. It was evaluated to about 10 nm when the probe was perpendicular to the surface under test.

The selected optical asphere was mounted on the air bearing table and scanned using the non-contact probe system. A set of 31 390 points was collected, as shown in figure 4(a), and analysed using the implemented minimax EPF and HTR fitting algorithms.

Table 5 illustrates results obtained using HTR and EPF as well as the *PV* value given by L_2 fitting. HTR provided more accurate results than EPF since PV_{HTR} (470.36 nm) was approximately 9 nm lower than PV_{EPF} (479.43 nm). The *PV* value given by L_2 (536 nm) was considerably higher than both other values which confirmed that L_2 overestimates *PV*. Similarly, to reference data, EPF takes approximately five times more execution time than HTR. Figure 4(b) shows the evolution of PV values given by EPF and HTR in function of execution time. Figure 4(c) represents the final residuals obtained using HTR. For all the above reasons, HTR proved its superiority for asphere and freeform minimax fitting.

Unlike L_2, minimax fitting can exactly estimate the formed error by directly minimizing the peak to valley (*PV*). Obtaining the exact minimum zone for profile or surface tolerance could be achieved at the expense of facility of the resulting mathematical formulation of the problem.

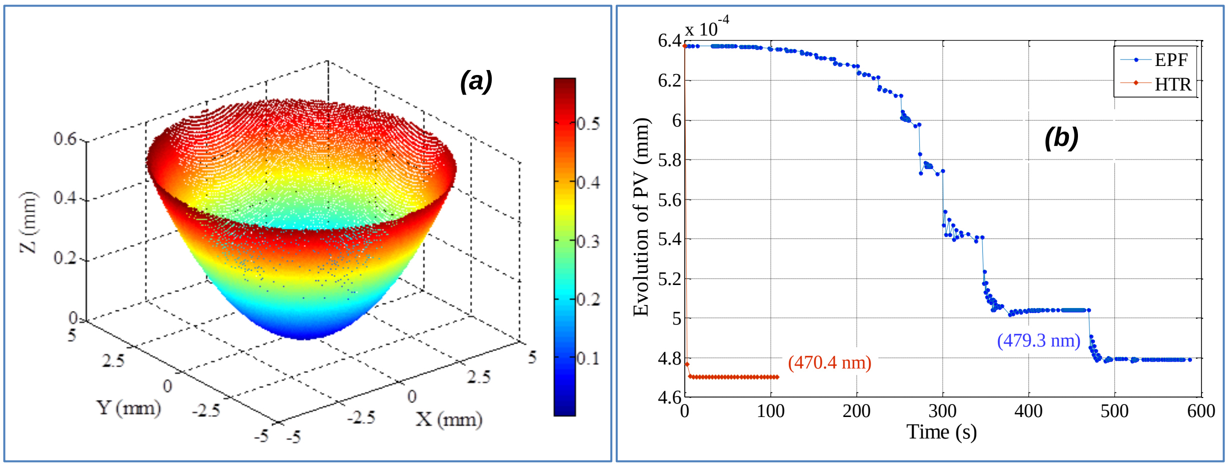

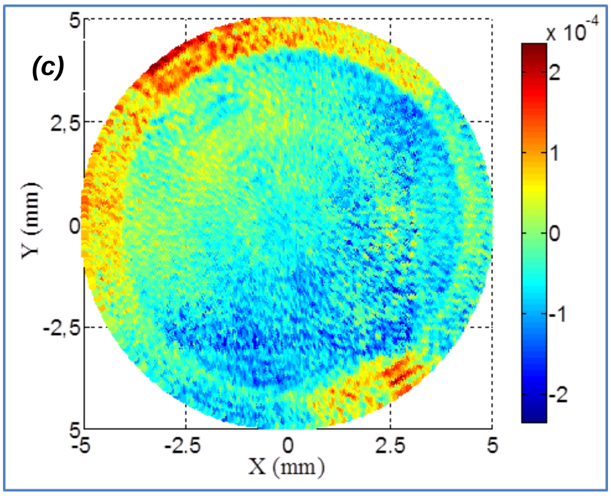

Figure 4: (a) optical aspherical lens: measured data using the ultra-high precision measurement machine (31 390 points), (b) Evolution of PV value for HTR and EPF algorithms applied on measured data (31 390 points), (c) optical aspherical lens: residual values (31 390 points).

Table 5: Comparison of HTR, EPF on measured data (31 390 points)

	Least squares (L_2)	Minimax (L_∞)	
		HTR	EPF
PV (nm)	536	470.36	479.43
Execution time *(s)*	10.23	107.69	586.96

<u>Conclusion</u>

The implemented HTR algorithm was first tested and validated using generated reference data sets based on Forbes method. Softgauges generation was conducted to obtain several shapes that simulate different conditions (number of points, deviation and slope). Results showed HTR superiority over EPF in terms of PV values and execution time.

Objective 2: Develop advanced techniques for data analysis

Since the measurement of freeform surfaces can be carried out with multiple sensors, the measurement data sets were transformed initially in the same coordinate system by a developed coarse and fine registration methods. Then a Gaussian Process (GP) model was built based on each of the two transformed data sets, followed by the maximum likelihood data fusion. Finally, the developed fitting algorithm was applied on the fused data for assessment of the minimum zone. The general workflow of the proposed method is illustrated in Figure 5. It can be seen that registration, data fusion and fitting are key methods.

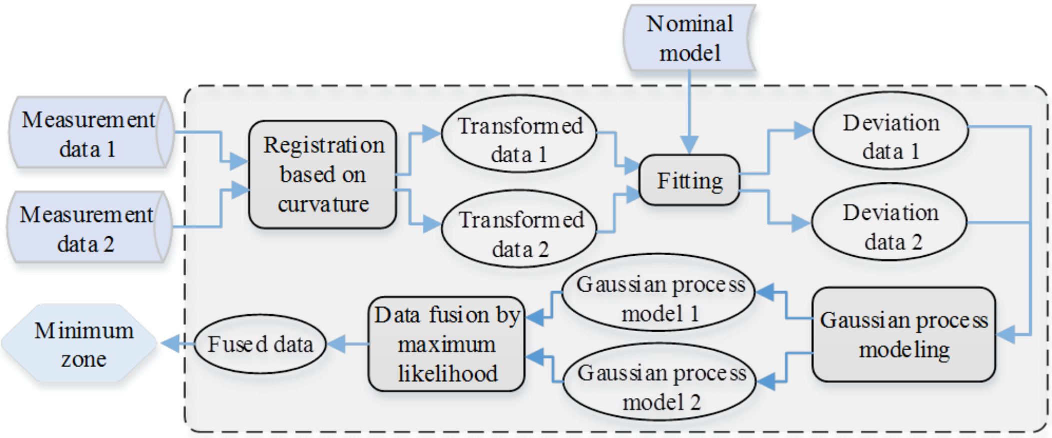

Figure 5: Illustration of the proposed method

The registration process aimed to determine the best alignment of two data types, Model data, (Q, the fixed set) and Scene data (*P*, the moving set) while combining them into the same coordinate system. Registration was essentially conducted in two steps including coarse and fine registrations. The coarse registration roughly aligned the two data sets with lower resolution from a global view. The resulting alignment was consequently optimized in the fine registration step for higher resolution.
GP approximation is a non-parametric fitting method. Based on a GP model, a surrogate model was built and adjusted to a more accurate model using experimental results obtained from simulations. Later, this work was extended to the Bayesian hierarchical GP model for integration of low-accuracy and high-accuracy experiments. In addition, a GP model was built to assess the form errors using coordinate measurements. Using a similar reference method, a Bayesian hierarchical model was developed, which combined misaligned metrology data of two different resolutions to evaluate their geometrical quality. A two-stage Multi-sensor Data Fusion model was proposed using GP models for dimensional and geometric verification.

Curvature-based registration

In coarse registration, two measurement data sets in different coordinate systems were initially aligned in the same coordinate system. Then, in fine registration, the matching vertex pairs in the two data sets were identified and the final registration parameters were obtained by minimizing the overall distance between these vertex pairs. Curvature was used to improve the efficiency and accuracy by matching vertices in both coarse registration and fine registration (Figure 6).

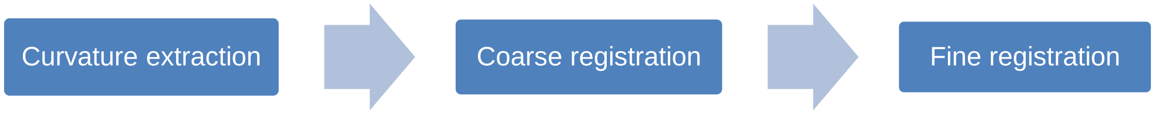

Figure 6: Curvature-based registration

Curvature definition and calculation

Curvature is an important attribute that measures the shape of a surface. It was calculated by the neighbouring points. Two curvature attributes, shape index and curvedness were used to describe the shape of a surface. The shape index and curvedness contains the local shape information equivalent to the pair of maximum and minimum curvatures or the pair of mean curvature and Gaussian curvature. Shape index specifies the shape type while curvedness specifies the size. The local shapes to which a vertex belongs were classified into 10 types.

Coarse registration using curvature-based Hough Transformation method

Since Hough transformation is based on exhaustive search, the computational complexity increases with the data volume. Therefore, curvature was used to reduce the number iterations in the searching process. Scene data and model data sets were registered employing the local frames built for all the vertices using Eigen vectors obtained by Eigen decomposition of the shape operator. The obtained transformation parameters were stored in the Hough table in ascending order according to the number of occurrences of each parameter. The best match was achieved when the similarities between transformation parameters were high enough.
In the classic Hough transformation, all the local transformation parameters between each vertex need to be calculated, which leads to considerable computational cost. However, curvature parameters were introduced to evaluate the degree of matching between the vertices first, in order to improve the efficiency. The shape index and curvedness of all the vertices were calculated and the shape types of all the vertices can be identified. The vertices with the same shape types were matched initially and the transformation operations were only executed between these initially matching vertex pairs.

Fine registration using curvature-based ICP method

The data sets were initially aligned in the same coordinate system and then fine registration was applied to all the vertices to determine the final registration parameters by minimizing the distance between two data sets. A comprehensive matching indicator combining both Euclidean distance and curvature distance was used for the proposed ICP method. After matching the vertices, the transformation parameters were calculated by solving a least square optimization problem. The objective function was defined with the combination of point-to-point (P-P) and point-to-plane (P-Pl) criteria.

Fitting

Fitting measured data to the nominal shape was a crucial step in assessing the form error of the manufactured part. Form error determination indicates the conformance of the manufactured shape to design tolerance specifications. For this, a variability function was defined. Among others, the PV, defined as the difference between maximum and minimum form deviations, was considered. The form deviation associated to the measured point P_i is its Euclidean distance to the nominal shape as shown in Figure 7.

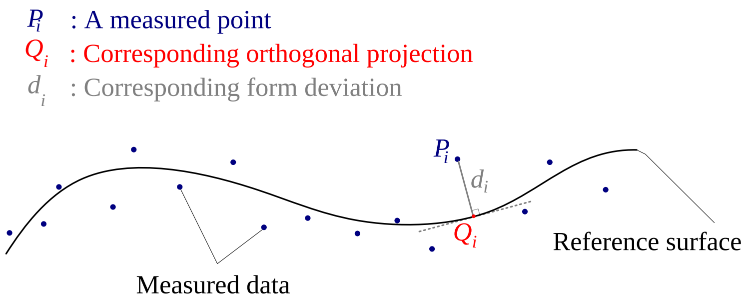

Figure 7: Definition of form deviations

Fitting measured data also required the selection of a fitting criterion, where Least squares and Chebyshev fitting are the most widely used. Each of these problems resulted in an optimisation problem with different mathematical properties. The PV returned by the Chebyshev fitting was the closest to the true value. However, this resulted in the optimization of a non-smooth objective function was more difficult than LS fitting. The minimum zone (MZ) fitting problem could be formulated as follows: Given a set of m measured data points $\{P_i\}_{1\leq i\leq m}$ and their corresponding orthogonal projections $\{Q_i\}_{1\leq i\leq m}$ onto a surface described using an implicit equation $f(\boldsymbol{q}, \boldsymbol{s}) = 0$ with $\boldsymbol{q} = (x, y, z)$ as the coordinates of a given point on the surface and $\boldsymbol{s}$ as the surface' shape parameters. The evaluation of the minimum zone value was conducted by means of an algorithm named the HTR algorithm.

Data fusion based on GP modelling and maximum likelihood

After registration, two data sets were transformed into the same coordinate system. Then data fusion was conducted on the two transformed data set in two steps. Both datasets contained the actual form deviations and the measurement noise; their noise scale was different. The fusion process aimed to effectively identify the actual form errors with reduced uncertainty and achieve a more reliable estimation of the minimum zone that is less sensitive to the noise. In the first step, the GP model with mean and uncertainty was built based on measured deviations of each transformed data set. The fused mean and uncertainty were estimated according to the maximum likelihood principle in the second step.

a. GP modelling of measurement data

GP proved to be an effective method to model the local random surface variation that exhibits the spatial distribution similarity. The measurement data is point cloud composed of vertices, can be treated as the superposition of the true manufactured shape of part and the measurement error. The deviations of the measurement data from the nominal part shape were extracted. Once the GP model is built, any prediction at new location can be obtained by the joint distribution of the measured value in Z-axis direction and the function value at the prediction locations.

b. Data fusion by maximum likelihood

The mean and the uncertainty of any vertex in the point was estimated by building the GP model for the two measured deviation datasets. Considering two measurement datasets, we evaluated the means and the uncertainties as m_1, m_2 and u_1, u_2, for the two datasets, respectively. Since the measurement noise is in Gaussian distribution, then the probability of both measurements getting result m was calculated as:

$$p\left(m \middle| m_1, u_1^2\right) = \frac{1}{u_1\sqrt{2\pi}} e^{-\frac{(m-m_1)^2}{2u_1^2}} \tag{6}$$

$$p\left(m \middle| m_2, u_2^2\right) = \frac{1}{u_2\sqrt{2\pi}} e^{-\frac{(m-m_2)^2}{2u_2^2}} \tag{7}$$

Then the likelihood of both two measurements getting m at specific position was:

$$p\left(m \middle| m_1, u_1^2, m_2, u_2^2\right) = p\left(m \middle| m_1, u_1^2\right) p\left(m \middle| m_2, u_2^2\right) = \frac{1}{2\pi u_1 u_2} e^{-\left[\frac{(m-m_1)^2}{2u_1^2} + \frac{(m-m_2)^2}{2u_2^2}\right]} \tag{8}$$

The corresponding natural algorithm was:

$$\ln\left(p\left(m \middle| m_1, u_1^2, m_2, u_2^2\right)\right) = -\left[\frac{(m-m_1)^2}{2u_1^2} + \frac{(m-m_2)^2}{2u_2^2}\right] + \ln\left(\frac{1}{2\pi u_1 u_2}\right) \tag{9}$$

Based on the maximum likelihood principle, we obtained the best estimation of m by maximizing (9). Therefore, we calculated the partial derivative of (9) to m as:

$$\frac{\partial \ln\left(p\left(m \middle| m_1, u_1^2, m_2, u_2^2\right)\right)}{\partial m} = \frac{\partial \left\{-\left[\frac{(m-m_1)^2}{2u_1^2} + \frac{(m-m_2)^2}{2u_2^2}\right] + \ln\left(\frac{1}{2\pi u_1 u_2}\right)\right\}}{\partial m} \tag{10}$$

By solving (12), we obtained the best estimated value as in 11.

$$\overline{m} = \frac{\left(\frac{m_1}{u_1^2} + \frac{m_2}{u_2^2}\right)}{\left(\frac{1}{u_1^2} + \frac{1}{u_2^2}\right)} \tag{11}$$

If we defined two weights, ω_1 and ω_2 as $\omega_1 = \frac{1}{u_1^2}$ and $\omega_2 = \frac{1}{u_2^2}$, then (11) can be written as:

$$\overline{m} = \frac{\omega_1 m_1 + \omega_2 m_2}{\omega_1 + \omega_2} \tag{12}$$

The uncertainty of $\overline{m}$ was calculated according to the uncertainty propagation principle as:

$$\bar{u} = \sqrt{\left(\frac{\omega_1}{\omega_1 + \omega_2} u_1\right)^2 + \left(\frac{\omega_2}{\omega_1 + \omega_2} u_2\right)^2} = \frac{1}{\sqrt{\omega_1 + \omega_2}} \tag{13}$$

Thus, the uncertainty after maximum likelihood fusion was smaller than any of two measurement datasets.

Tests and validations on simulated data

The simulation was conducted on an aspheric optical part whose shape is generated with certain control parameters. A set of 5025 grid points were sampled in the 2D space and their coordinates (x, y) were used to calculate the values of r. Hence, the nominal shape of the part was generated by setting the parameters as:
R=9.127x10^{10}, K=-1, a_4=1.589x10^{-5}, a_6=7.922x10^{-10}, a_8=-1.859x10^{-11}, a_{10}=-1.859x10^{-15}. The actual form deviations were generated following a predefined mathematical equation given as: $f(x, y) = \cos(0.0025x) + \cos(0.0025y)$. Figure 8 illustrates the generated nominal part surface as well as the simulated form deviations.

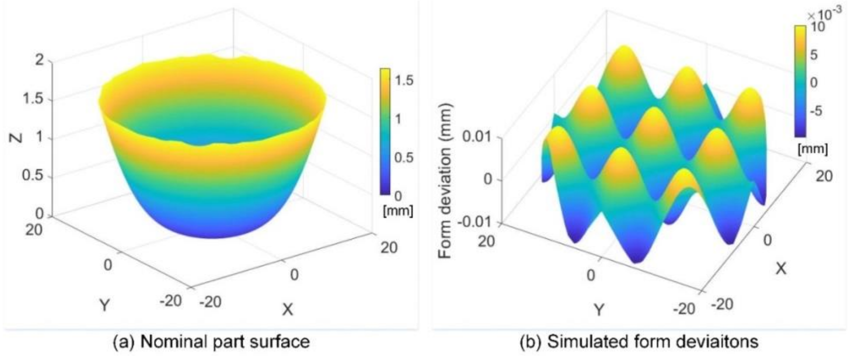

Figure 8: The nominal surface and form deviations of the simulated part

To account for the measurement errors, noise was added to the simulated form deviations. To emphasize the discrepancies between the two measurement datasets, their noise scales were specified differently. The noise was generated with zero-mean Gaussian distribution. For one dataset, the noise was generated at 503 points randomly sampled from the 5025 with $\sigma_1 = 0.0002$. This dataset was intended to imitate data collected from a tactile probe, which had better accuracy but lower number of sample points. For the other dataset, the noise was generated for all the 5025 points with $\sigma_2 = 0.002$, imitating data from a scanning device, which had lower accuracy. The resulting distribution of coupled form deviations and measurement errors of both datasets can be visualized in figure 9.

The GP models of both datasets were derived based on the simulated datasets. The GP models were further used to make predictions on all the data points. Figure 10 shows the mean prediction and prediction interval of the GP model for measurement data 1. The mean prediction reached a close fitting to the real form deviations after training with the noisy data, and the 95 % prediction interval almost fully enclosed the noise, indicating the accurate capture of the uncertainty. The average range of the prediction interval was 0.0078 mm. Similarly, the results of measurement data 2 are illustrated in figure 11. With a subset of only 10 % of the training data points as used in measurement data 1, the GP model realizes an accurate prediction on all the other points. Since the noise scale used for this dataset was smaller, the prediction interval was narrower compared with dataset 1, reaching an average range of 9.113×10^{-4} mm.

Data fusion was conducted based on the mean and variance predicted by the two GP models at each point. The mean prediction and prediction interval of the fused model is shown in figure 12. After data fusion, the average range of the interval falls to 7.3125×10^{-4} mm, which was smaller than those of both datasets before fusion. It could be concluded that, through GP modelling, the actual form deviations can be captured among the measurement noise, even with a small number of sample points. And through data fusion, the uncertainty of both GP models was reduced, which facilitates filtering out the noise in data and the robust assessment of the form deviations.

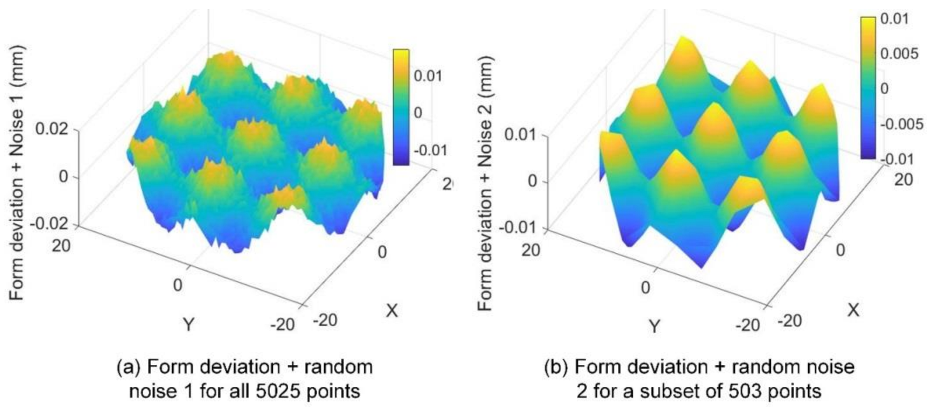

Figure 9: Form deviation and generated noise for two simulated measurement datasets

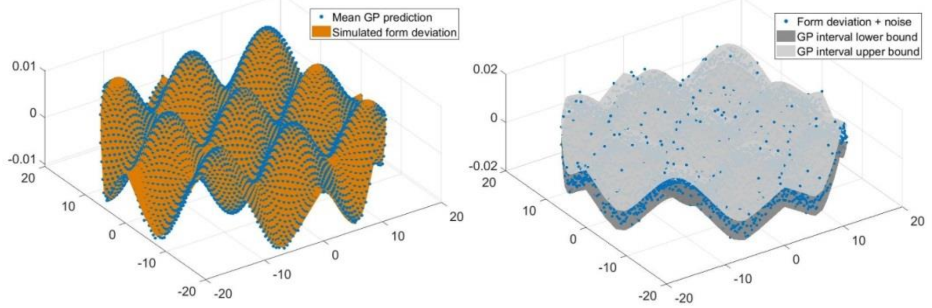

(a) Mean GP prediction of the real form deviations

(b) GP prediction interval fitting the noisy data

Figure 10: Mean prediction and prediction interval of the GP model for measurement data 1

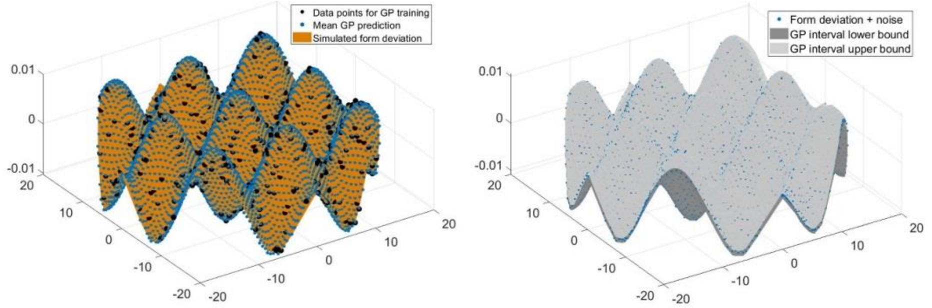

(a) Mean GP prediction of the real form deviations

(b) GP prediction interval fitting the noisy data

Figure 11: Mean prediction and prediction interval of the GP model for measurement data 2

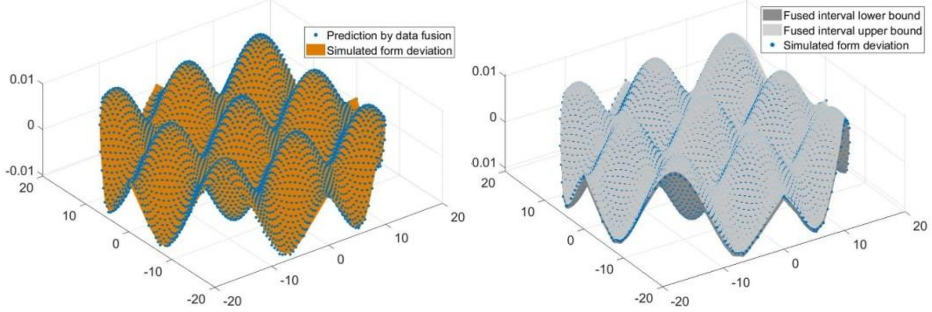

(a) Prediction of form deviation after data fusion

(b) Prediction interval after data fusion

Figure 12: Mean prediction and prediction interval of the data fusion model

Conclusion

Aspheric and freeform optical elements have many advantages compared to regulate spherical lenses, however those advantages are closely linked to their geometry quality in term of form deviation. Thus, an accurate measurement of the form deviation of aspheric and freeform optic parts is highly required. Furthermore, it must be taken into account that the measurement of aspheric and freeform optic parts generally requires the use of multiple sensors. As a consequence, data processing is a major source of potential error in the process of measurement. Data processing becomes more complex and a crucial step to the assessment of the form deviation.

A review of literature shows that multi-sensor data fusion has been investigated. Nevertheless most of the developed methods and algorithms failed when they are applied to aspherical and freeform optics. Thus a generic and global approach for data treatment of multi-sensor metrology has been introduced combining three steps: registration, fitting and data fusion. The novel framework introduced is based on the Peak to Valley quality indicator for the form deviation assessment and start with a registration step based on curvature computation. Then we have introduced a min-max fitting method for form error assessment and finally a data fusion method integrating Gaussian Process models and maximum likelihood estimation. The feasibility of the developed framework was demonstrated through simulation data and also real measurement data of a designed artefact.

Objective 3: Design, manufacture and characterise innovative aspherical and freeform optical reference elements

Th work carried out under this objective involved the defining and manufacturing reference thermo-invariant standards (aspherical and freeform optical surfaces) made of thermo-invariant materials. These reference standards were calibrated using ultra-high precision measuring machines (accurate single point or imaging instruments) and the calibration traceability has been carefully established. The realisation of reference surfaces suitable for low uncertainty traceability of asphere and freeform metrology instruments answers a central need of industry.

Developed metrological reference surfaces (MRS standards)

Zerodur and Super invar were selected as preferred materials, based on their physical properties and machinability.

In total, six optical artefacts (summarized in table 6) were manufactured. Four of them are reference thermo-invariant optical standards - Metrological Reference Surfaces (MRS standards). MRS standards comprise one asphere ("Classical asphere") and three freeform surfaces. Additionally, two mathematics-based surfaces were manufactured and used for the calibration of algorithms for nominal shape fitting.

The calibration procedure and some results are presented. MRSs were characterized in terms of surface roughness and surface form including radii measurement. The calibration involved surface form measurement followed by post processing in order to traceably extract nominal form deviation. It can be useful to describe the surface form by a mathematical function that has the best fit to a series of the measured cloud of data points.

Table 6: Summary of MRS and their properties

	Freeform I	Freeform II	Freeform III	Classical Asphere	Mathematics-based surface I	Mathematics-based surface II
Type	Two radii	Toroid (convex)	Toroid (concave)	A50-40HPX-U-S	Aspheric form with additional steps	Freefrom surface
Calibration instrument	TWI PTB	TWI PTB	TWI Mahr	TWI Mahr	Ultra-high precision profilometer at LNE	Ultra-high precision profilometer at LNE
Material	Super invar	Super invar	Super invar	Ohara S-LAH64 black coating of backside	Zerodur	Zerodur
Machining	SPDT	SPDT	SPDT	subaperture polishing	Magnetorheological Finishing (MRF)	Magnetorheological Finishing (MRF)
Size (diameter)	40 mm	50 mm	100 mm	50 mm	45 mm	50 mm
Marker	none	4 gaussian peak markers with different depths: 0.5 µm to 1.25 µm	none	2 gaussian peak markers by ion beam (one placed out of clear aperture)	none	none
Form description	Two radii: 39.5 mm and	Two different radii on	Two different radii on	Even Asphere: R=31.075 K=-0.744	Even Asphere: R=9.127 x10^{-40} K=-1	Freeform described using an explicit equation.

	40 mm	orthogonal axes: radius 1: 40 mm, radius 2: 42 mm, overall best fit radius: 40.9 mm	orthogonal axes: radius 1: 400 mm, radius 2: 450 mm, overall best fit radius: 420.6 mm	A4=4.36 x10^{-7} A6=-2.27 x10^{-10} A8=-1.70 x10^{-13} A10=-3.68 x10^{-17} A12=8.94 x10^{-22} A14=1.85 x10^{-23} A16=-6.27 x10^{-27}	A4=1.278 x10^{-9} A6=7.922 x10^{-16} A8=-1.859 x10^{-18} A10=1.733 x10^{-21} + 9 steps	
Mount	Morse taper	Morse taper	Morse taper	Glued on D25 holder	No holder	No holder

The impact of mounting on the MRS's optical surface form was studied by means of finite element method (FEM) simulations and subsequently experimentally verified. It was found that a Morse taper was most suitable if the specimen must be measurable with and without a holder.

One example of MRS was the two-sphere MRS (Freeform I) (Figure 13). The surface combines spherical segments with different radii of curvature (39.5 mm and 40.0 mm) with cosine transition in between. All spherical segments have the same vertex in the centre.

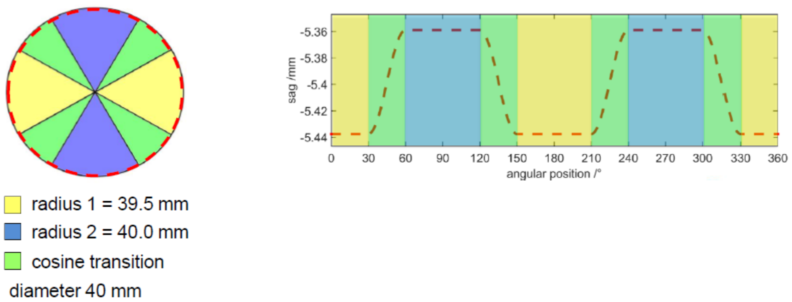

Figure 13: Nominal shape of Freeform I

The advantage of freeform 1 was that the form and radius of its spherical segments can be calibrated by classical measurement techniques. The measurement results for the sphericity are shown in Figure 14 on a measured aperture with a diameter of 34 mm. The surface quality of the specimen should be improved for the Fizeau interferometer to reach its uncertainty of 11 nm (k=2), otherwise the confocal position cannot be determined with sufficient accuracy.

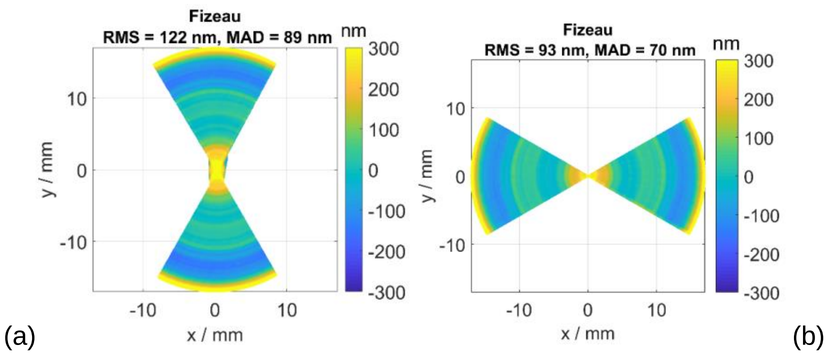

Figure 14: Measurement results of the sphericities of Freeform I (aperture with 34 mm diameter) measured with a Fizeau interferometer at PTB. (a) shows the sphericity of the two segments with design radius R_1 = 40 mm. (b) shows the sphericity of the two segments with design radius R_2 = 39.5 mm.

To initially characterize the manufactured artefacts, it can be useful to describe the measured surface form using a mathematical function, that has the best fit to a series of the measured data points for the reference measurement data of the MRS. Such procedure is called functional description within this report. Different functional descriptions were tested to describe the nominal surface forms in space as well as the measured data sets.

For example, for such a non-rotationally-symmetric optical surface like freefrom I, one possible representation were the Zernike polynomials. They were developed to describe wavefront errors. The characterization is based on limited radial distance (corresponding to the aperture). Another disadvantage of the Zernike polynomial representation is that the coefficients depend on a sampling grid and a selected aperture for the Zernike polynomials (diameter on which the polynomials are defined). Some Zernike coefficients depend on position and tilt of the surface.

The Zernike polynomials were used to fit the reference measurement data for freeform I (two-radii). We used the Zernike coefficients definition according to ANSI Standard with n_{max} describing the maximum radial order and m_{max} describing the maximum angular frequency. The residuals for different maximum polynomial orders are shown in Figure 15. The RMS values of the residuals amount to 317.98 nm, 96.76 nm and 43.29 nm. Even with the very high number of polynomials n_{max}, m_{max} = 45 leading to 1081 polynomials, still a significant residual remained.

To overcome the disadvantages of the Zernike polynomial representation, the use of different representation that combines radial and axial coordinates separately from a position and a tilt of surface was proposed by CMI. Details about this method can be found in the "Guide about the calibration procedure of the developed innovative thermo-invariant asphere and freeform metrological reference surfaces".

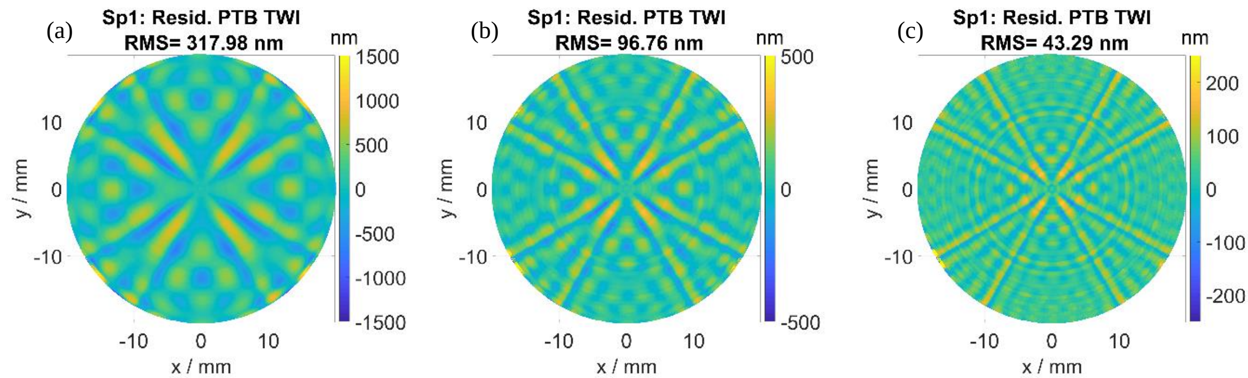

Figure 15: Residuals after fitting Zernike polynomials with different maximum polynomial orders to the reference measurement data (PTB/TWI) of freeform I: (a) maximum polynomial order of n_{max}, m_{max} = 18 (190 polynomials), (b) maximum polynomial order of n_{max}, m_{max} = 30 (496 polynomials), and (c) maximum polynomial order of n_{max}, m_{max} = 45 (1081 polynomials).

The extended algorithm was applied to freeform I (two-radii surface). It has a two-fold symmetry (2 sections per cycle). The RMS value of the residuals decreased with increasing number of coefficients. The RMS value of the residual amounts to 39 nm and only 41 coefficients were used for the model. Therefore, the results were much better than using Zernike polynomials to fit the measurement data of freefrom I (Figure 16).

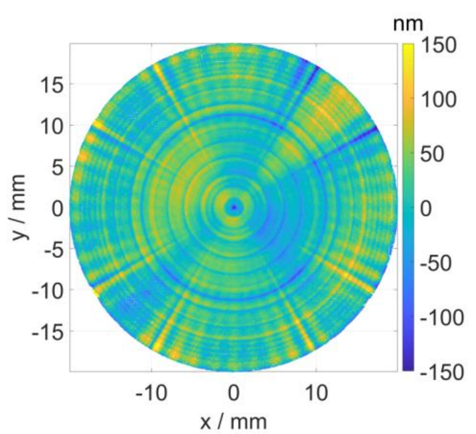

Figure 16: Residuals after fitting the reference measurement data for freeform I (PTB TWI) to the new model proposed by CMI.

For measuring the radii of the two-sphere MRS (and other specimens), the radius measuring technique was improved further within the project and compared between the partners. One cat's eye and two confocal positions must be determined. For this purpose, two goniometer stages having the centre of rotation close to the common vertex were added.
The radius bench was developed further to make uncertainties of 100 nm or less possible (for single full spherical segments). The uncertainty was dependent on the specimen (lens) parameters as well as on the measurement conditions (including temperature variations) during data registration. It should be noted that the result corresponds to a best fit sphere on the aperture and thus will vary if a different aperture ratio is used. The deviation from the best fit sphere in the centre has to be determined and corrected for. Therefore, a sphericity measurement should always be performed. In this case, and in particular for diamond turned surfaces, care has to be taken that the lateral resolution is sufficient for the structure in the centre of the specimen. Thus, the stage for specimen movement must be of sufficient quality. Quantitative stage specifications can be derived from the radius range to be measured and the aperture ratio defined by the available lenses and the specimens.

Developed mathematics-based surfaces I and II

The first mathematics-based surface corresponds to an aspherical surface, as specified in ISO 10110-12, combined with nine steps projected along orthogonal directions. The steps and the aspherical surface were combined. The role of the added steps was twofold. First, it was considered as an artificial added form error to illustrate the departure from the ideal asphere. Second, they materialise the upper and lower surfaces defining the MZ. As a result, during the process of fitting measured data, the locations of the significant points defining the MZ were approximately known a priori. The theoretical amplitude of the steps, which was equal to 7 µm, was selected according to the manufacturing process. In fact, this was the smallest amplitude realised using the considered manufacturing technique. The final obtained optical surface represents neither axis of symmetry nor degrees of invariance (figure 17(a)).

The proposed freeform surface (figure 17(b)) is described using the explicit polynomial equation in (14). This surface has an application in the domain of virtual reality. To represent a freeform, the proposed artefact has no degree of invariance. The amplitude of the artefact was taken to be equal to 7 µm. This choice was made according to the manufacturing process constraints. The shape parameters are given in table 7.
Three different materials were used for manufacturing of MRS (see In total, six optical artefacts (summarized in table 6) were manufactured. Four of them are reference thermo-invariant optical standards - Metrological Reference Surfaces (MRS standards). MRS standards comprise one asphere ("Classical asphere") and three freeform surfaces. Additionally, two mathematics-based surfaces were manufactured and used for the calibration of algorithms for nominal shape fitting.

The calibration procedure and some results are presented. MRSs were characterized in terms of surface roughness and surface form including radii measurement. The calibration involved surface form measurement followed by post processing in order to traceably extract nominal form deviation. It can be useful to describe the surface form by a mathematical function that has the best fit to a series of the measured cloud of data points.

Table 6): Super invar, Ohara glass and Zerodur. The selection of material was based on their physical properties and machinability. Super invar 32-5 is an alloy (Ni-31.75%, C-0.1%, Mn-0.4%, Si-0.1%, Co-5.4%, Al-0.1%, Cu-0.1%. Zerodur - a lithium-aluminosilicate glass-ceramic has CTE = 0.05 x10^{-6} K^{-1} and for glass Ohara S-LAH64 holds 6.1 x10^{-6} K^{-1}.

$$z = a_1(x^3 + y^3) + a_2(xy^2 + x^2y) + a_3(x^5 + y^5) + a_4(x^4y + xy^4) + a_5(x^2y^3 + x^3y^2) - a_6x - a_7y - a_8 \tag{14}$$

Table 7: Shape parameter a_i values for mathematic-based surface II

Parameter	Value
$\boldsymbol{a_1}$	9.792 x10^{-7}
$\boldsymbol{a_2}$	4.940 x10^{-7}
$\boldsymbol{a_3}$	-6.310 x10^{-10}
$\boldsymbol{a_4}$	-3.086 x10^{-10}

a_5	2.551 x10^{-10}
a_6	3.087 x10^{-4}
a_7	3.087 x10^{-4}
a_8	-6.876 x10^{-10}

(a) *(b)*

Figure 17: Nominal shape of Mathematics-based surface I (a) and II (b).

Form characterization of MRS

The forms of all artefacts were initially measured with their corresponding reference measurement system in order to characterize the form accuracy, test the developed algorithms and check if the design descriptions should be adapted to another model description (see below). Figure 18 shows the measurement results for the six artefacts.

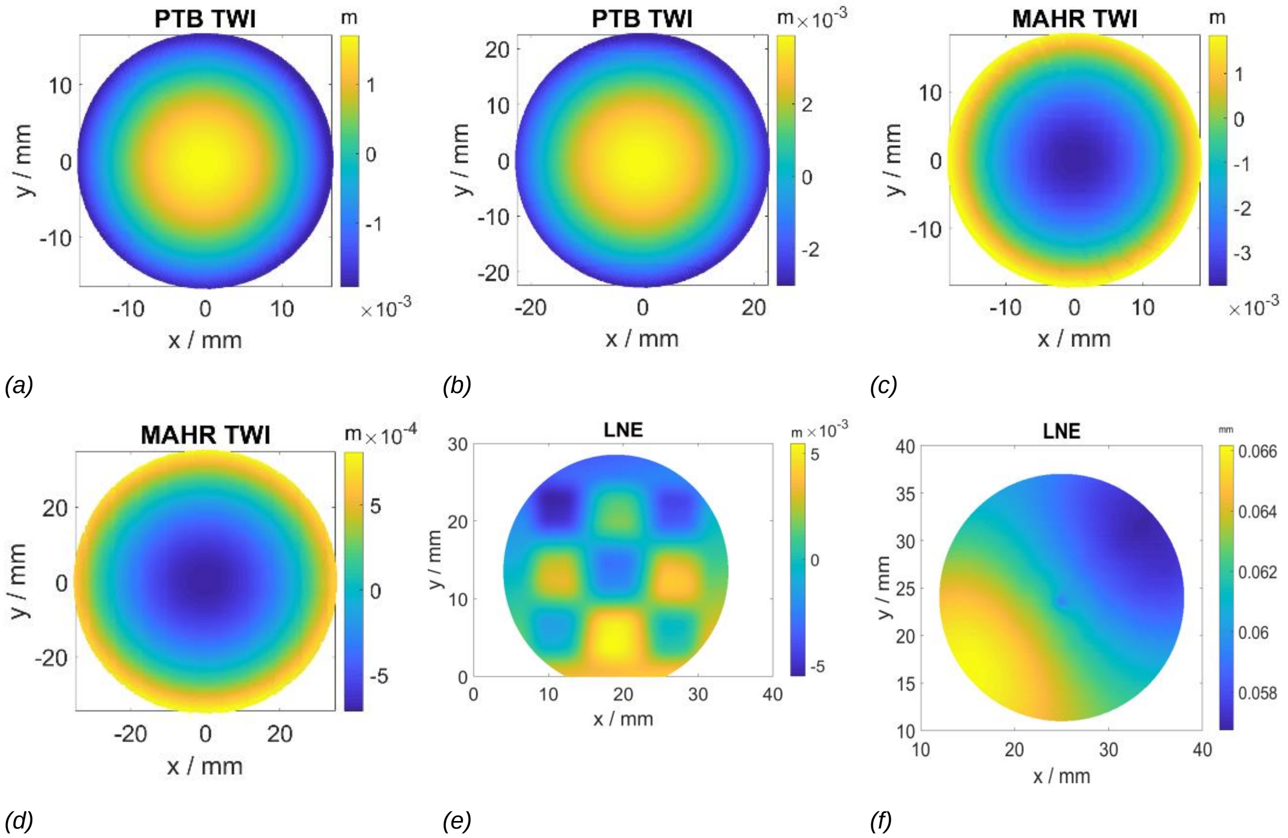

Figure 18: The figure shows the form measurement results of the reference measurement systems for all six artefacts: form of freeform1 measured with TWI at PTB (a), form of freeform2 measured with TWI at PTB (b), form of freeform3

measured with TWI at Mahr (c), form of classical asphere measured with TWI at Mahr (d), form of mathematics-based surface I and II ((e) and (f)) measured with LNE's ultra-high precision profilomter.

Conclusion

The design and manufacture of innovative aspherical and freeform reference optical elements, made of thermo-invariant material, was successfully performed. For the two-sphere MRS, a first calibration chain was facilitated for the transfer of traceability from NMIs to stakeholders. Interlaboratory measurement comparisons of the form measurements of the metrological reference surfaces were performed by the project partners and stakeholders. The results were discussed within the consortium and as an output, partners and stakeholders gained insight about their measurement systems and their performance on freeform surfaces. The uncertainty for the radius measurements was improved to 100 nm or less.

The mathematics-based surfaces I and II were manufactured by a Magnetorheological (MR) finishing process and measured using LNE's high-precision profilometer. The Hybrid Trust Region algorithm was used to analyse the obtained data. The resulting PV value was compared to the one specified in the design. Results showed that the mean deviation of obtained PV values to the theoretical MZ value was 641 nm. This deviation was due to the long duration of the manufacturing process (9 hours). Measurements of the second artefact gave a mean value of PV that were equal to 766 nm. The obtained results allowed to perform inter-laboratory comparisons as well as the testing of implemented minimum zone fitting.

A guide about the calibration procedure of the developed innovative thermo-invariant asphere and freeform metrological reference surfaces was written and it can be downloaded from the project website.

Objective 4: Improve measurement capabilities of NMIs and DIs on aspherical and freeform standards

This objective aimed at substantially enhancing the existing precision metrology for aspherical and freeform optical surfaces, such as to reach a reference metrology level. The improvement of metrological infrastructure includes imaging and single point scanning measurement principles. Each of the two approaches has its advantages and disadvantages.

Optimization of full field measurement technology: Tilted-Wave Interferometer (TWI)

To optimize full field measurements with the tilted-wave interferometer (TWI), two fundamentally different simulation tools were developed and compared by USTUTT and PTB. The simulation of the highly complex experiment is very important for this measurement device, since the measurement process itself is based on a numerical forward model of the instrument.
Since some differences were found in the first comparison of results from the simulation tools at PTB and USTUTT on the base of phase difference comparisons, comprehensive investigations were performed.
For comparison, several test cases were defined: The comparisons were performed using a design model of the TWI (corresponding to a perfectly calibrated system) and performing simulations for different surfaces under test (SUTs) in different conditions. Differences between the two simulation tools became apparent and were investigated in detail within the project.

As a result, several issues were identified and solved: The refractive indices of both simulation tools as well as the pixel coordinates were defined differently and were adapted to each other as well as to the real-world systems. Further comparisons have shown that the different approaches of the two simulation environments still caused differences between the simulated optical path lengths in the range of a few nanometres. The model used at USTUTT was based on a black box model of the TWI and the nominal optical path lengths were calculated from Zernike polynomial functions that are defined in two reference planes. The model used at PTB was based on a physical model of the TWI (lenses, lens positions, etc.) and the nominal optical path lengths were calculated by tracing rays through the optical system. The investigations showed that even though the Zernike polynomial fit errors were well below 1 nm in the reference planes, this can lead to nanometre scale errors for a complete measurement simulation under certain circumstances. By increasing the upper limit of the Zernike development, the differences between the simulated optical path lengths were reduced to the sub-nanometre range.

Figure 19 shows the differences between the simulated optical path length differences of PTB and USTUTT for the first test case at the beginning of the investigations (left panel). In the right panel of Figure 18 the same result is shown after the differences have been eliminated and the degree of the Zernike polynomial functions used for the black-box model has been increased. The results show that the differences between the simulation tools could be improved by two orders of magnitude down to the sub-nanometre level. The good correspondence of the results also serves as verification of the two different simulation systems.

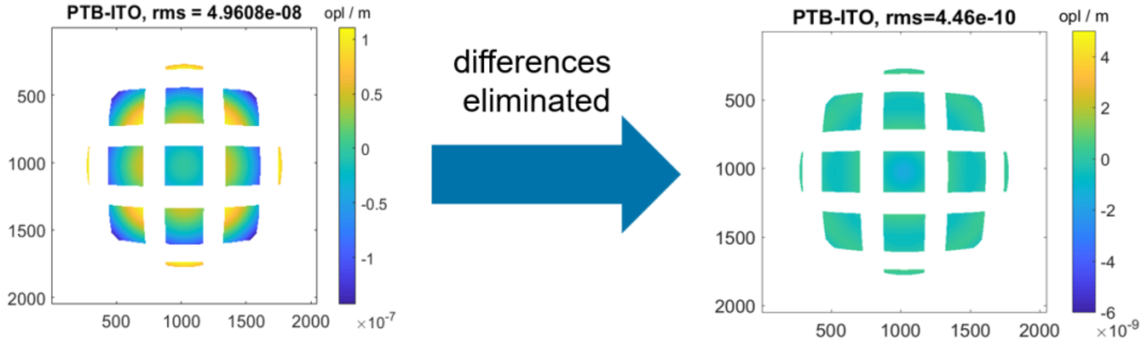

Figure 19: differences between the simulated optical path length differences of PTB and USTUTT under initial conditions (left panel) and after elimination of model differences and improvement of parameterization (right panel). The RMS error of the differences could be reduced to sub-nanometre range.

The improved model was the basis for Monte Carlo simulations performed by USTUTT and discussed with PTB in order to investigate the impact of positioning errors on freeform surface measurements. For this purpose, the simulation tool developed by USTUTT was used.
The positioning of specimens in the Tilted Wave Interferometer was done with a high precision stage (6 axis hexapod). Although it worked very accurately, small positioning errors in the range of a few microns were unavoidable. Therefore, the evaluation algorithm solved both for the surface error and the specimen's position. Its performance was investigated in order to derive possible optimization strategies.
Nine exemplary test cases were chosen, consisting of three nominal surface shapes and three different surface errors that were added to each nominal shape. The nominal shapes are defined as follows:

1.) Classical asphere (description see Table 6)
2.) two-radii specimen (FFI, R_1=40 mm, R_2=39.5 mm, diameter 40 mm, see Table 6)
3.) toroidal surface (FFII, R_v = 40 mm, R_h = 42 mm, diameter 50 mm, see Table 6)

The three different surface errors are depicted in Figure 20.

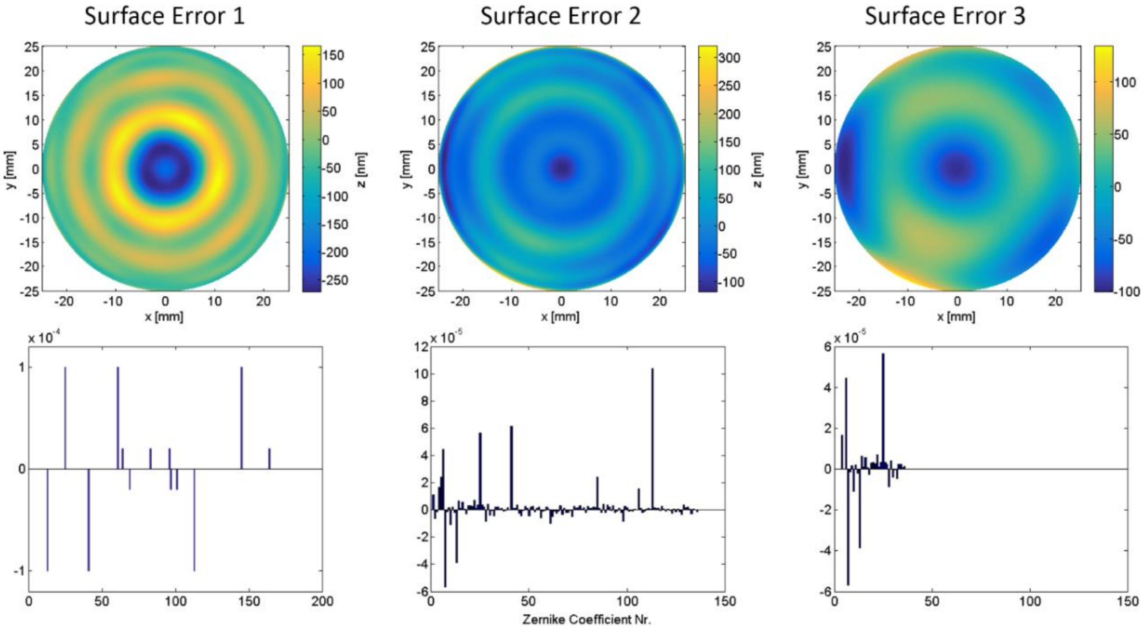

Figure 20: Surface errors which were used for the simulation of freeform surface measurements. The first row shows the errors as two-dimensional false colour plot. In the second row, the corresponding Zernike coefficients are shown.

We used the Zernike coefficients definition according to Malacara with Zn being the n-th coefficient. Surface error 1 consisted of 13 Zernike polynomials with Z164 being the highest order coefficient (chosen Zernike polynomials: see Figure 20), simulating mid spatial frequency components that are not covered by the standard 136 Zernike expansion that is used in the algorithm to fit the low frequency part of the surface.

Surface error 2 is the Zernike fit of a real measurement, consisting of all Zernike polynomials up to Z136. Surface error 3 was created using surface error 2 but using only Z5 to Z36. To simulate misalignment, the nominal position was changed by adding or subtracting up to 10 µm in each axial direction and introducing a rotation error of up to 0.35 mrad per tilt axis.
Results have shown that the misalignment in z was most critical, whereas positioning errors along x and y as well as rotational errors were reconstructed well (typical: sub-micron). In one test case a fundamental ambiguity shows: Surface error 2 contains astigmatism, but the difference between the toroidal surface at its nominal position and a rotated position can also be described by astigmatism. Since the algorithm tries to minimize the error by altering the specimen's position, the astigmatism of the surface error is misinterpreted as misalignment in this case.
This problem is known from sphere measurements. Here the ambiguity lied between defocus and a radius error. Also, a tilt term from misalignment cannot be distinguished from a tilt term due to a surface's shape error. For aspheres and freeforms this ambiguity is more complex and especially freeform misalignment can lead to a variety of features that could also be a form error from the manufacturing. The only way to overcome these ambiguities is knowing the position of the surface absolutely.
For the development of a strategy for decreasing uncertainty due to positioning errors, different approaches were discussed between PTB and USTUTT. For further investigations it was decided to add absolute knowledge of the measurement position by external measurement.
One strategy was to measure the absolute distance between the last surface of the objective and the surface under test during calibration as well as during measurement of the SUT.
The improvements that can be achieved by including the absolute knowledge of the measurement position using an external measurement were investigated by PTB with the help of virtual experiments. To this end, the SimOptDevice simulation tool was used to simulate TWI measurements. In agreement with USTUTT different test cases were defined to assess the achievable improvement when the absolute measurement position is known. The test cases included different design topographies (sphere, two-radii specimen (FFI), toroidal surface (FFII)), different design deviations, with and without camera noise, with and without different amounts of misalignment, and different measurement positions.

The results (Figure 21) showed that the knowledge of the distance between the last surface of the objective and the surface under test improved the results significantly.

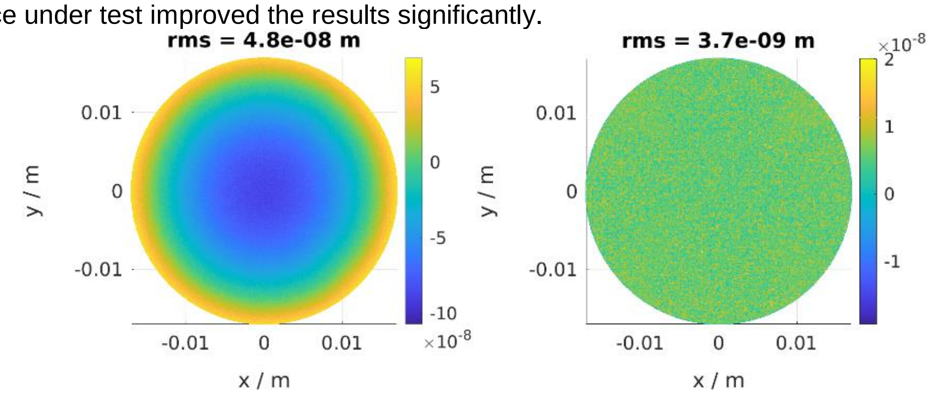

Figure 21: Residual reconstruction errors for the test case with the following data: two-radii specimen (FFI), measurement position z = 8.859 mm ((distance from last surface of objective), with deviation from design based on a measured point cloud of SMD which was fitted by a Zernike polynomial function of order n= 15, camera noise with standard deviation of 10 nm, misalignment Δx, Δy, Δz = 7 µm. The left figure shows the residual reconstruction error for the standard reconstruction case. The result on the right was achieved using an additional measurement of the specimen's z-position.

The results of the simulation study were discussed with USTUTT, IPP and VTT. To implement the optimal strategy, PTB recommended to integrate a white light interferometer. The best way was to integrate it into the experimental setup at USTUTT to measure the absolute distance between the last surface of the objective and the surface under test (during measurement and model calibration).
The white-light interferometer Optisurf UP was chosen and borrowed from Trioptics by PTB and USTUTT and integrated into the breadboard setup at USTUTT. The absolute information about the distance between the specimen and the last surface of the interferometer can be measured in this way.
The former reconstruction method was divided into two main steps: At first, the form (low and mid spatial frequencies) was reconstructed. In a second step, the high frequency errors were reconstructed. This current method had some disadvantages: First, it was a more-step procedure, which was necessary to reconstruct the form as well as the high-frequency errors. Furthermore, the point density on the surface under test was

not uniformly distributed over the x- and y- coordinates and depended on the local slopes of the surface under test and its measurement position. To investigate an alternative reconstruction method by applying the methods for calculation of the Jacobian matrices developed in EMRP IND10, virtual experiments were conducted at PTB. The new developed reconstruction method consists of only a single reconstruction step and the distribution of the point density was chosen freely. The new method was implemented by PTB and was tested using virtual experiments to generate test data using the design model of the TWI (corresponding to a perfectly calibrated measurement system). The results showed that the new method is a promising approach for TWI data evaluation because a high frequency reconstruction result with an equally distributed point density at the surface under test can be achieved in a one-step reconstruction procedure.

Finally, new concepts for calibration of the TWI model were investigated during the project. One approach was the reduction of the calibration positions. For this purpose, an analysis of the sensitivity matrix was conducted. The sensitivity matrix is part of the inverse problem that is solved within the calibration algorithm. Multiple position sets have been assessed and promising sets were also tested experimentally. It was shown that with an optimized set of calibration positions the measurement time during the calibration process was reduced to approximately 40 % without any negative impact onto the uncertainty of the measurement results. For many calibration procedures, as it had been the state of the art for the TWI, calibration spheres are widely used. In contrast to that, we investigated the use of non-spherical calibration specimens. As there were two calibration spheres in use during the established procedure, three configurations were examined: Replacing one sphere with a non-spherical object and continue using one of the two calibration spheres (two configurations) and replacing both spheres with non-spherical elements. Monte Carlo Simulations were performed and showed improved results, especially for the third option (two known non-spherical objects).

Advanced calibration strategy for the multi-wavelength interferometer (MWI)

Calibration strategy for multi-wavelength interferometer (MWI) developed within the project has two main parts. A software package including numerical model of the system and position compensation was developed. Two approaches were tested for the numerical model: Fourier based propagation using wave optics approximation and Snell's law-based propagation using geometrical optics approximation. Due to time requirements and sufficient accuracy, the ray-based approximation was used by default. The nominal model of the arrangement was improved by measurement of calibration artefacts with known shape. Further, algorithms working on least square manner to compensate position error of the measured elements were developed.
Testing of the software package was executed in two steps. In the first step the same aspheric element (80 um departure from best-fit-sphere) was moved in different positions close to best fit sphere confocal position and the deviation from nominal surface shape was measured (Figure 22). The repeatability was computed as standard deviation (STD) between all measurements. Peak to valley (PV) of the STD map is 21 nm. In order to verify measurement accuracy, a cross test with calibrated machine (ASI-QED) was performed with the deviation of 4 nm RMS (root-mean-square) and 55 nm PV.

MWI was equipped with automatic motorized 5-axis optical bench having Incremental Rotary Encoders (IRC). However; to increase the positioning accuracy and to measure absolutely, the system was upgraded to add linear and rotary optical encoders. Better accuracy and precision of the positioning system improved capabilities of stitching interferometry as well as calibration strategies. The linear axes were calibrated using laser interferometers available in CMI. The complete system including rotary axes was calibrated using trigonometric measurement under different conditions followed by error separation technique.

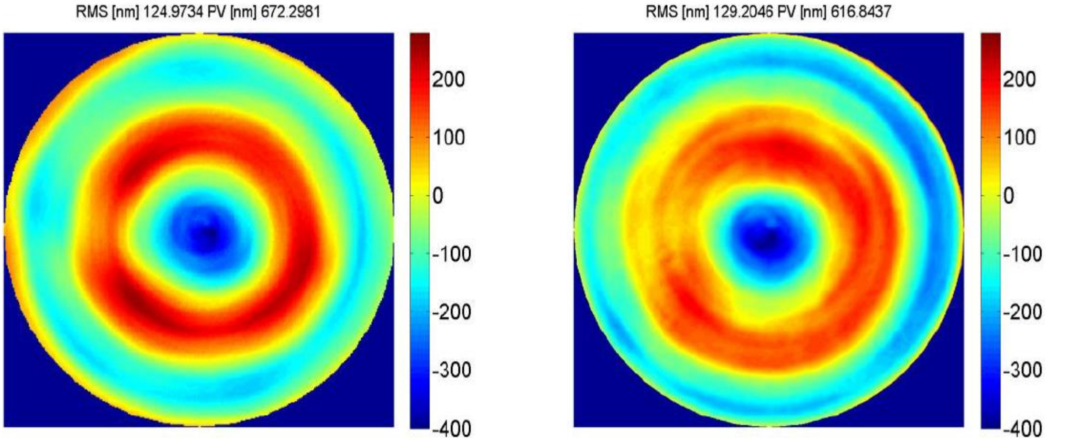

Figure 22: Measured form deviation from nominal surface on aspherical element by reference device (left) and by MWI (right).

The sub-aperture stitching software package was developed. It is based on an innovative approach that converts stitching task to a system of linear equations which can be solved as the least square problem. Using the linear algebra theory this task was solved directly without any iterative computation and therefore the computation time was in order of seconds for tens of subapertures. The algorithm was successfully tested with several measured data sets of spherical surfaces with diameter up to 200 mm. A stitching mismatch error is ordinarily below 5 nm. After upgrade and re-assembling of MWI, the stitching SW package was tested on aspherical and freeform elements.

Ultra-high precision multi-sensor optical profilometer

A novel multi-sensor optical profilometer for measurement of freeform samples was built at VTT. This allowed measuring several types of samples.
Before the project the only optical interferometer at VTT for cm class samples was a Fizeau interferometer for flat optics. The slope range for such device however limits its use for mirrors and other flat samples. VTT also had a scanning white light interferometer (SWLI) for measurement of freeform samples with sizes up to 5 mm. The multi sensor profilometer allows measurements of samples similar to SWLI but sizes up to 10 cm with only small degradation of vertical precision.
Prior to this project, VTT built a 2D optical interferometer to be used as an optical CMM. The translators and interferometers are used as base for the 3D profilometer as they allow precise and straight movements of the sample block (figure 23(a)). During the project, VTT incorporated the measuring heads of existing BrukerGT-K scanning white light interferomoter and a chromatic confocal sensor (micro epsilon) into the setup in order to build a multi sensor profilometer capable of spanning large areas.
A three-legged design was selected for the support structure of the height sensors in order to have best possible stability. The support features height adjustment range of 10 cm in order to place large samples into measurement volume without damaging the sample or the measurement heads. The chromatic confocal sensor was located 30 mm from the SWLI sensor and the measurement planes of the sensors can be adjusted into same height. This allows measuremetns of samples using both sensors without touching the sample between measurements.

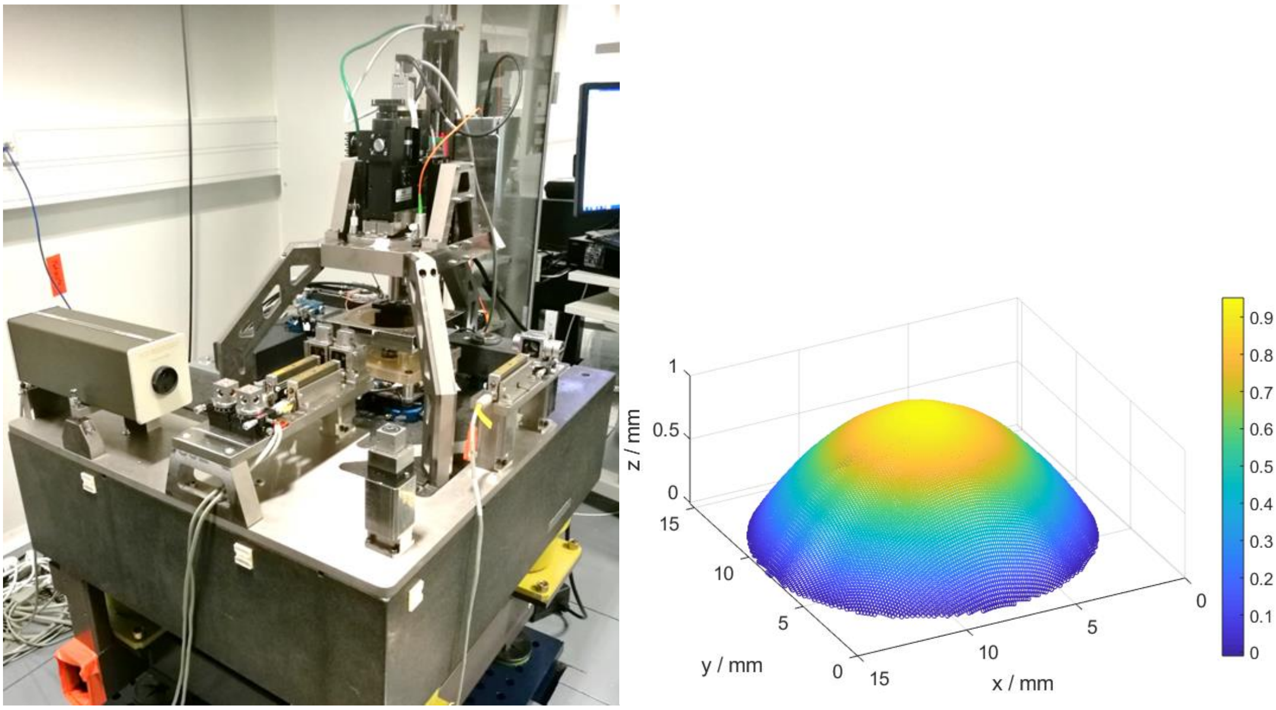

Figure 23: (a) The VTT multi-sensor profilometer, (b) 3D-profile of a printed optics sample measured using confocal microscope from the centre of the lens

In the test of the flatter samples using low magnification stitching accuracy of better than 10 nm was achieved. In the stitched dataset it was clearly visible that some of the residual error was due to tilting of the sample during motion, as there was an almost perfectly aligned area in the middle of the seam. On tests made with more rounded samples using 20x objective the stitching errors on highly tilted areas were slightly larger. In these tests datasets of up to 300 sub-imaged could be combined into one dataset.
The profilometer reached the designed accuracy of 30 nm at samples with small height differences using the SWLI sensor head. Using the confocal sensor the accuracy was similar for mm class samples and slightly worse for flat samples.

<u>Calibration of 3D surface transfer function in CSI and advanced coating technique</u>

Imaging of smooth, highly curved or tilted surfaces is recognized as one of the most challenging and unsolved problems for optical surface measuring techniques, such as imaging confocal microscopy (ICM) and coherence scanning interferometry (CSI). The main reasons are 1) the steepness of the features causes large angle reflection or high order diffraction that cannot be captured by the lens; 2) optical aberrations in the imaging system degrade the performance and lateral resolution of the system.
Measurement and correction of the 3D surface transfer function (STF) for a CSI instrument was proposed and thorough examination of the method demonstrated that it is possible to calibrate the 3D STF of a CSI system by measuring a precision microsphere which has a diameter much larger than a wavelength (Figure 24). The inverse filtering of the 3D STF can effectively improve accuracy of CSI measurements of surfaces that feature varying slopes and spatial frequencies.

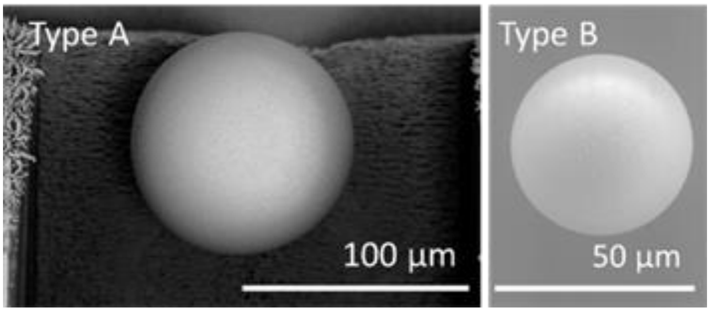

Figure 24: Calibration microspheres

To improve the accuracy of CSI surface measurements, the inverse filtering was applied to the raw fringe data to correct optical measurements of three manufactured surfaces with varying slopes and spatial frequencies. For example, two sinusoidal surfaces (R521 and R525) were measured, which have pitches of 15 µm and 135 µm and amplitudes of 1.6 µm and 19 µm, respectively. The result was inversely filtered and compared with the corresponding stylus measurement, as shown in figure 25.
The 2π errors in the original CSI measurements were effectively removed and the corrected CSI results agree with traceable, contact stylus measurements with an RMS height difference in the order of a few tens of nanometres across a 170 µm field of view. Careful calibrated CSI systems and interference microscopes can conduct surface topography measurements with nanometre-level accuracy. This technique developed by UNOTT significantly enhances the measurement accuracy and slope range of optical 3D measurement instruments for freeform surfaces.

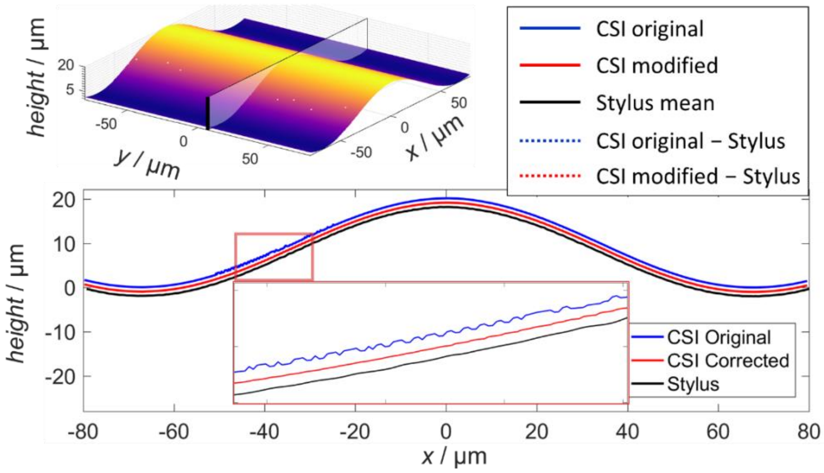

Figure 25: Comparison of the CSI and stylus measurements of R521.

Furthermore, UNOTT collaborated with HIT (Stakeholder) and developed a method, called fluorophore-aided scattering microscopy (FAM), to overcome the low signal-to-noise ratio and detectability that are caused by high surface slopes in ICM. The detected signal was significantly enhanced with the aid of fluorescence due to the scattering by the surface now being more isotropic, i.e. the number of back-scattered photons is increased. Using the fluorescence method UNOTT were able to visualize specular silicon wafer samples with slopes greater than 81° significantly greater than the theoretical maximum measurable slope of 24°. The coating and FAM techniques that were developed showed promising results for improving the metrological capability for measuring freeforms with high slopes. This approach may also be used with other organic or inorganic fluorophore materials, since biocompatibility is not required for engineering surfaces.

Inter-laboratory comparison and results

Two inter-laboratory comparisons of measurements on aspherical and freeform surfaces were conducted at LNE and PTB. The comparison organised by LNE was made based on the obtained form errors obtained using a MZ reference fitting algorithm (HTR). A number of partners participated to the inter-comparison and carried out measurements using different traceable measurement capabilities. The procedure includes the different components of the metrology of aspherical and freeform surfaces (ultra-high precision measuring machines, thermo-invariant material measures and reference algorithms). Measurements were made on two selected thermo-invariant material measures (TIMM-1 and -2) shown in Figure 25. TIMM-1 (Figure 26-a) was designed for the assessment of MZ fitting of aspherical surfaces while TIMM-2 (Figure 26-b) was designed for freeform surfaces.

The obtained value of MZref for TIMM-1 is equal to 6.303 µm with an associated expanded standard uncertainty of 2 nm. The average MZ and expanded standard uncertainties obtained from measurements are respectively equal to 6.305 µm and 5 nm for LNE, and 6.303 µm and 2 nm for UNOTT. These two measurements could be considered as the most accurate. Measurements on TIMM-1 made by all participants present a good agreement as shown in Figure 27. These results prove the capabilities of all participants to carry out measurements on aspherical surface with high accuracy.

Based on the obtained results of MZref, a deviation from the theoretical value of MZ (MZth = 7 µm) by 697 nm can seen. The deviation (MZth - MZex) is due to the manufacturing process. Thus a small error in the estimation of the wear rate of the tool used in the MR process may lead to significant form errors. The manufacturing of TIMM-1, because of its complex shape, took approximately nine hours while a normal MR cycle takes fifteen to forty-five minutes, which may explain this deviation.

A good agreement between the obtained results was observed. The expanded standard uncertainties on the weighted mean value of the MZ for the two material measures does not exceed 16 nm.

Unlike TIMM-1, the obtained MZ values for TIMM-2 are more dispersed. The obtained MZref value is equal to 0.768 µm with an associated expanded standard uncertainty of 16 nm. The MZ values are plotted in figure 28. The measurement made by LNE has the lowest expanded standard uncertainty (24 nm).

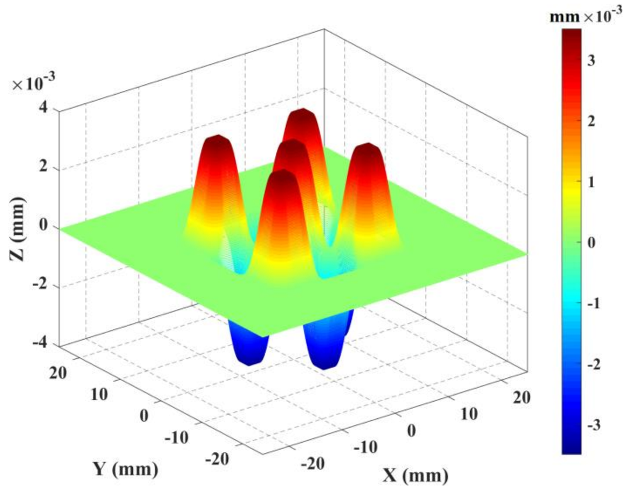

(a) TIMM-1 (b) TIMM-2

Figure 26 Design of the thermo-invariant material measures for freeform surfaces

The obtained results show the interest of the design of the thermo-invariant material measures for MZ fitting. Both optical and tactile measuring systems provide results with good agreement. However, the obtained values are still highly sensitive to the presence of outliers among the collected data. Hence, clear pre-processing steps for filtering and outlier removal must be defined.

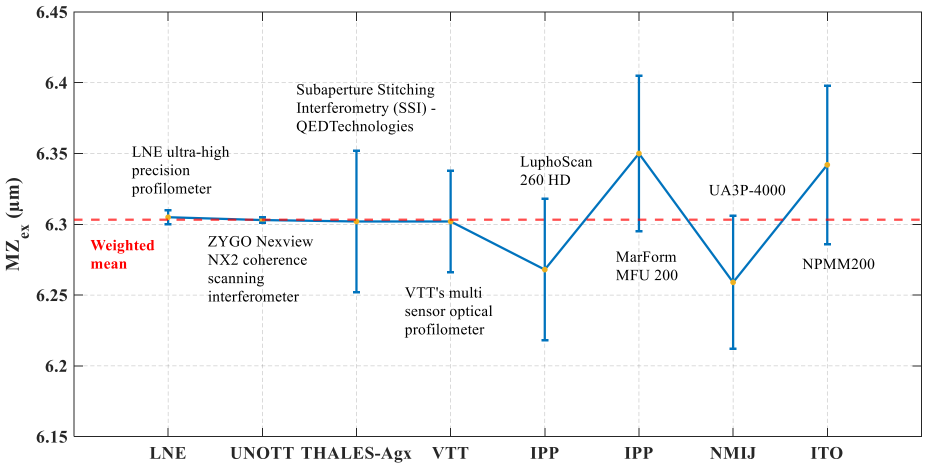

Figure 27: Obtained MZ values for TIMM-1

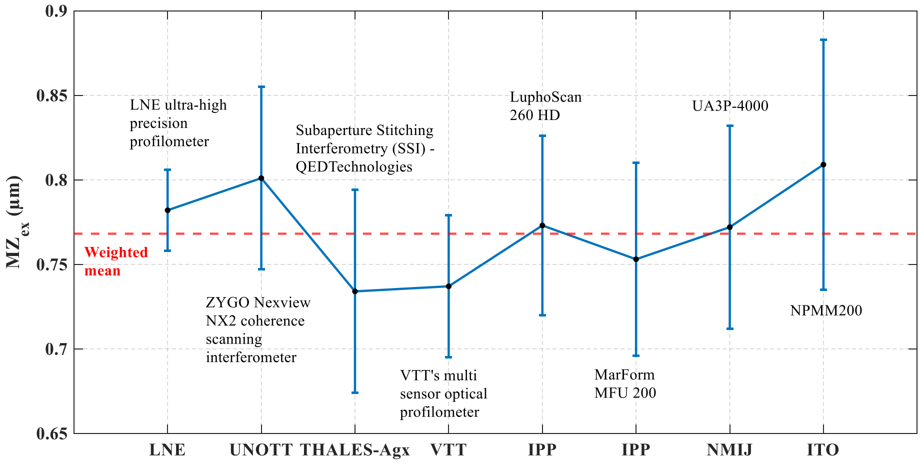

Figure 28: Obtained MZ values for TIMM-2

<u>Conclusion</u>

Some of the developments carried out during the project are summarized in table 8.

Table 8: List of improved metrological capabilities

Partner	Developed capability	Type
PTB	simulation tools were developed to optimize full field measurements with the TWI, comparison with USTUTT	improvements to existing equipment
USTUTT	simulation tools were developed to optimize full field measurements with the TWI, and comparison with PTB	improvements to existing equipment
IPP	improvements to full field measurements using MWI, in collaboration with USTUTT, PTB and CMI	improvements to existing equipment
VTT	Multi sensor profilometer was built, and the characterization of the new instrument	New device
UNOTT	extending measurement capability of confocal sensor and CSI to high slopes	improvements to existing equipment
SMD	further developed the confocal probe for their Zeiss F25	improvements to existing equipment

Objective 5: Develop a strategy for the long-term operation of the capability developed

The goal of this objective was the development of a strategy for the long-term operation of the capability developed, including the take up of the technology and measurement infrastructure developed by the project. For this purpose, two case studies on the application of the developed reference fitting algorithms and on the improvement of the metrology chain for innovative 3D printed precision freeform optics was performed.

<u>Case study I: application of the developed reference fitting algorithms</u>

a. Description

Reference fitting algorithms are needed so that users of optical measurement devices can analyse their data with reliable algorithms. The complex shapes of freeform samples call for new methods for defining differences from nominal surfaces. As an example, typical measurements of height differences only might be misleading due to high slopes and curvatures. Therefore, the project developed reference minimum zone and least squares fitting algorithms. Additionally, the reliability of new algorithms can be established by referencing softgauges fitting algorithms as well as testing them against the reference algorithms.

This methodology was followed to generate a number of reference data sets that are accessible to all project partners and that are also published at the project's website to give open access to industry and other interested parties (https://www.ptb.de/empir/freeform-home.html).

The same scheme was applied to assess a fitting algorithm developed at the CMI. The set "Reference Data 1" was used for the validation. The corresponding exact value of Minimum Zone was equal to 0.005 mm and the applied transformation is as follows: a rotation around X-axis of π/30, - π/30 around Y-axis and a vector translation of [0.05, -0.02, 0.1]. The layout of the generated reference data is given in Figure 29.

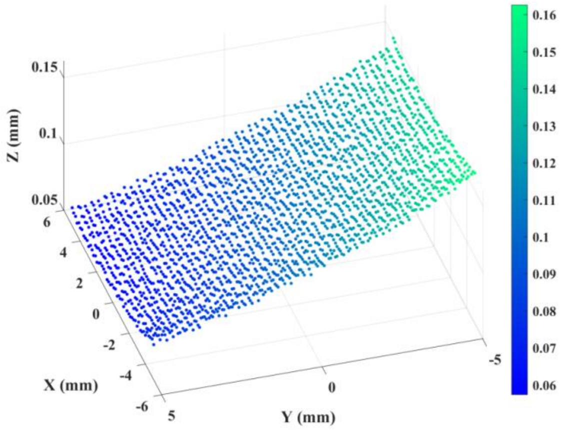

Figure 29: Layout of the generated reference data

b. Result and analysis

The obtained result of Minimum Zone by the algorithm under test was equal to 0.005389 mm and the obtained transformations are given in table 9.

Table 9: Obtained transformations using the algorithm under test

Total translation (original position of vertex has opposite sign)		
x[mm]	y[mm]	z[mm]
-0.06797	-0.07916	-0.09925
Rotation matrix at vertex (transpose this orthonormal matrix for the inverse transformation)		
0.999999	7.1E-08	-0.00157
-1.3E-05	0.999965	-0.00836
0.001568	0.008356	0.999964

Based on these results, a statement about the acceptance or the rejection of the algorithm could be made. However, LNE can only provide the accuracy of the tested algorithm without specifying if the algorithm can be accepted or rejected. The acceptance or rejection of a developed algorithm depends on the application. The developer and the user of the algorithm should agree about the acceptance criteria and LNE can only certify the calculation errors of such algorithms.

Case study II: improvement of metrology chain for innovative 3D printed precision freeform optics

3D printing allows faster prototyping and manufacturing of customized goods combined to previous production methods. However, earlier quality of such methods has not been up to the task for optical components. Iterative 3D printing technology (Printoptical® technology) allows manufacturing of optical components without any need for post-processing (polishing, coating or painting). This technology is under development in the Institute of Photonics at UEF (in collaboration with the inventor and manufacturer: a Dutch/Belgium company LUXeXceL). It will be highly suitable for several applications such as medical devices, safety, energy, telecommunications, aerospace, etc. In particular, the 3D printing technology may represent the future of ophthalmology, including 3D printing of eyewear (artificial lenses, glaucoma valves, etc.). As the accuracy of printing needs iterative corrections to reach the desired quality, methods for fast validation of the manufactured samples are needed. As the printed material is relatively soft and even small scratches need to be avoided, optical characterization methods are preferred.

a. Design of the selected optical freeform

The selected freeform was designed to produce structured lighting (stripes of decreasing width) from a point source (figure 30). The freeform was roughly parabolic with 27 mm diameter and 3 mm thickness. The lens surface modulation consists of shallow grooves with varying width in order to create the desired light pattern.

Figure 30: design of 3D printed optical freeform

b. 3D printing of the selected freeform

UEF utilizes Printoptical® technology, proprietary to LUXeXcel, which is a form of industrial inkjet printing process using UV-curable polymer material. The UV-curable resin is injected through thousands of nozzles of an inkjet printhead layer-by-layer basis in such a way that a single pass covers the entire printing area. Contrary to other 3D printing processes that inherently suffer from large surface roughness the Printoptical® technology consistently provides smooth surfaces due to careful control of the curing process. The surface form accuracy is a bigger challenge, and most of the UEF research and process development have been aimed to improve this. The printer stationed at UEF deviates slightly from the current line of LUXeXcel printers that are designed for printing ophthalmic lenses.

A drop-on-demand printing technique was employed with a series of modified ink-jet printer heads that have a nozzle droplet volume of 2.6 pl and print layer thickness of 4 µm. The printing took place layer by layer and, in order to solidify the droplets, we used a UV-curing lamp.

The basic 3D printing process, described in detail by Assefa et al. [4] is a layer-by-layer ink-jet printing technique, where three printheads (each with 1000 parallel nozzles, all three printheads slightly misaligned to triple the resolution) deposit 17 µm diameter droplets of liquid polymer on the substrate. Adjacent droplets merge after deposition before curing, forming a layer with a thickness of around 1 µm (depending on how many droplets overlap when letting them to spread and merge before curing) and shape defined by the (sliced) printing data. The deposited layer is solidified by UV exposure, and subsequent layers are grown using the same procedure one by one until a staircase approximation of the desired surface is formed. The outer printed surface can be smoothed by controlling the fluid dynamics during UV-curing throughout the lens build-up process. As a result, the 3D printed optical element is complete without any post-processing, like polishing or coating to reduce the surface roughness.”

c. Measurement methods and reasons for selecting the used methods

The goal of the case study was to print the selected freeform lens closer to design specifications than would be possible without iterative manufacturing. The diameter of the lens was 27 mm and its thickness amounts to 3 mm. In this study, only the quality within the inner area of the lens with a diameter of 13 mm, height range of 1 mm and tilt range (for the smooth areas) of 15 degrees was studied for simplicity (Figure 31).

Figure 31: 3D printed lens used in the case study

A two-phase iterative technique was used. After the first 3D printed freeform optics was printed by UEF and measured at VTT, the next iterations were compared to the result of the first iteration. This was achieved by using a Mach-Zehnder interferometer at UEF for the measurements to check if the results of the newer iterations were corrected towards the design goal (aided by the measurement errors of the first iteration). Here, the sample iteration n+1 was compared to iteration nVTT to see the changes between the sample shapes. Within this process, the printing parameters were adjusted until the difference between the iterations n and n+1 is the same as the difference of the measured profile of n and the specifications. Then, the best manufacturing result of UEF in iteration n+1 was send to VTT and measured at VTT using a multi-sensor 3D profilometer. If the measurement result of VTT did not fulfil the desired form accuracy, the sample was sent back to UEF and the 3D printing process was optimized again using the measurement results of VTT. This process was repeated until the form of the 3D printed freeform optics was accurate enough to fulfil the requirements.

d. Results and analysis

Three iterations of the lens were printed, two samples of each iteration. There was significant decrease in deviation from specifications after three iterations (Figure 32). The maximum measured deviations from the design profile in the central 13 mm area of the lens decreased from ±45 µm to ±35 µm to ±3 µm in iterations a, b, and c. The shape of the specimen, after some iteration, was quite similar, down to µm class in all iterations.

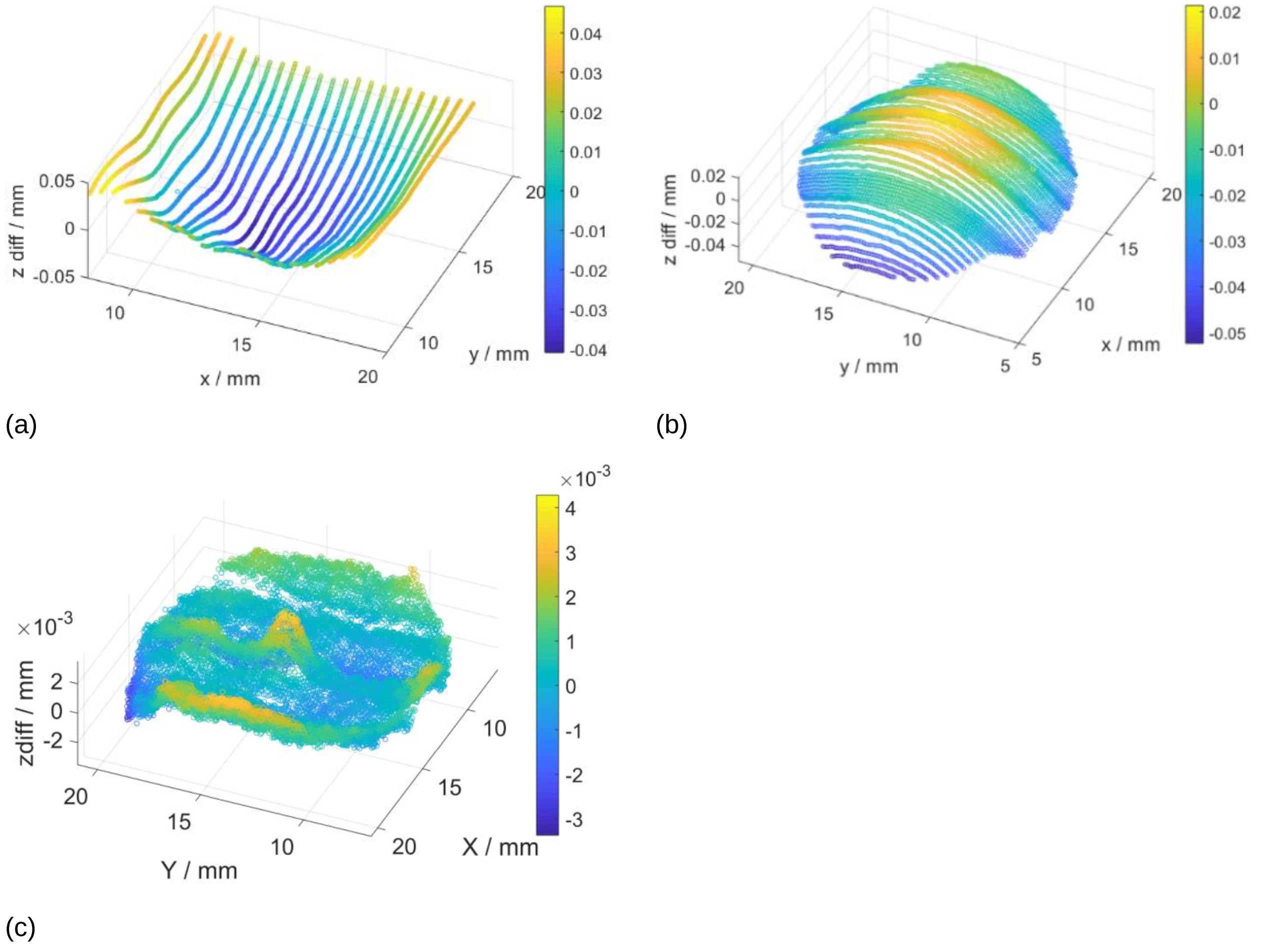

Figure 32: Deviation from specifications of iterations 1 (a), 2 (b) and 3 (c) measured using a chromatic confocal probe. The last iteration was measured with higher resolution to see if any defects were missed.

The developed algorithms allowed to test how the measured data from optical freeform measurements differ from designs. Also, soft gauges were developed for testing new fitting algorithms and comparing their results to reference algorithms without the need for measurement data.

Metrological capabilities developed within the project were used to perform iterative manufacturing of 3D printed freeform optical components. The iterative manufacturing allowed the production of a freeform lens with the desired accuracy close to the repeatability of the 3D printer. The final iteration was measured to be within ±3 µm from the specifications. The case study highlighted the need for a fast print-measure-print cycle for best results. The printing and measuring techniques tested in the case study were found to be sufficient to the task with some limitations. However, a slightly faster measurement procedure and performing the measurements on the production site were optimal.

5 Impact

A stakeholder committee was established which includes five members. The stakeholder committee signed a Non-Disclosure Agreement, and has been invited to attend the progress meeting and to provide assistance and recommendation to the project partners. The members of the stakeholder committee had access to the project website's member area. The stakeholder committee ensured that the results and expertise are relevant to users of asphere and freeform optical elements.

The consortium disseminated knowledge and results on the project's webpage, and through participation at international conferences, input to standardisation committees, organization of workshops and trainings as well as publications in peer reviewed and trade journals. 12 papers were already published in different peer-reviewed journals e.g. Journal of the European Optical Society, Precision Engeneering, Optics Express, Optics Letters; and 4 papers are drafted and submitted. Furthermore, partners have given 42 presentations at national and international conferences/workshops/interest group meetings in the area of freeform optical surfaces including e.g. EUSPEN, ASPEN/ASPE and Macroscale.

Impact on industrial and other user communities

This project aimed to improve the metrological capabilities within the optics area to support the industrial community. The reference least-squares and min-max fitting algorithms, and reference surfaces that have been developed in this project can be directly used by the user communities. These outputs will also improve the capabilities of the metrology machines used in the measurement of aspheres and freeform surfaces. All end users from the photonics industry will be able to harmonise their work on a high level.

The uptake of the results from this project will lead to the production of more accurate asphere and freeform surfaces in industry and research laboratories, which will exhibit higher and more advanced functionality and application. These advancements will enhance the traceability chain for all optical systems, such as consumer imaging systems, industrial imaging systems, lithography optics and many other high-end systems in astronomy and linear accelerators.To reach this aim, the outputs of the project were shared with Soleil (synchrotron), Essilor, DisgitalSurf, Mahr, Mitutoyo, Asphericon, Bruker and Thales-Agx by email and lateral visits. LNE and ENS Cachan developed reference algorithms for min-max fitting and generated several softgauges for the verification of commercial software. Discussions have been held between ENS Cachan and the companies DigitalSurf about the use of reference softgauges. Further discussions were conducted between LNE, PTB and NPL concerning the use of reference sauftgauges. Thales Agx is benefitting from the metrology developed in this project to improve their optics manufacturing process. Mahr collaborated with PTB and USTUTT for the improvement of the TWI technology. PTB measured the two radii artefact made of thermo-invariant material with the TWI and compared the sphericities in the spherical segments to the results of a Fizeau interferometer. These results are important for the traceability of TWI measurements. Furthermore, PTB and USTUTT developed and compared different simulation software for the TWI. UNOTT developed a new method for calibrating the 3D transfer function of coherence scanning interferometry. This technology can be used by Zygo, Alicona, etc. VTT developed a new multi-sensor profilometer for measuring large freeforms, which has already been used to measure samples from customers. Additionally, PTB, IPP and LNE developed metrological reference surfaces (MRS), made of thermo-invariant material, that are available for calibration services. Those MRS were used in themeasurement comparison between the partners of the project.

Furthermore, participants from several industrial companies and research centres attended the training on: optical metrological reference surfaces, accurate measuring aspheres with TWI and radius measurement which was organised by USTUTT and PTB. Results of the project were regularly presented at the High Level Expert Meeting (CC UPOB) which has members from industry and research institutes, as well as at theSpecial Interest Group Meeting: Structured & Freeform Surfaces SFS-EUSPEN annual meeting and the 1st International Workshop On Optical Freeform organised in Paris. About 100 particpants attended the SFS-EUSPEN and more 50 particapants arrented the 1st International Workshop On Optical Freeform.

Impact on the metrology and scientific communities

The significant improvement of the measurement capabilities will have immediate metrological impact through comparison measurements between NMIs. The artefacts used for the comparison have been selected after analysing the technical requirements suitable for the measuring instruments involved in the project. Furthermore, a test procedure, describing the measurement procedure, data acquisition and data handling has been prepared. For the effective comparison of the datasets, the data comparison software was developed. The evaluation methods and results of this round robin included three optical freeform surfaces made from a temperature-stable material, Super Invar. The freeforms had diameters of 40 mm, 50 mm and 100 mm and best-fit radii of 39.75 mm (convex), 40.9 mm (convex) and 423.5 mm (concave). The freeforms were measured by means of different optical (pointwise and areal) instruments as well as a tactile measuring instrument. For comparison, the bilateral pointwise differences between the available measurements were calculated. The root-mean-square values of these differences ranged from 15 nm to 110 nm (neglecting spherical contributions) and provided an insight into the status of typical freeform measurement capabilities for optical surfaces. The results of the inter-laboratory comparison measurements for three metrological reference surfaces have been submitted to a peer-reviewed journal. These international comparison measurements ensure that NMIs and recognised research laboratories benefit from the achieved results by strengthening their scientific knowledge of asphere and freeform metrology and unifying the international metrology methods for such surfaces.

Additionally, two case studies applying the project’s results have been investigated. One case study focused on the application of reference algorithms and reference softgauges and the other case study on 3D printed freeform optics. VTT planned the case study on 3D printed freeform optics with UEF. In this context, the possibilities and limitations that 3D-printing can offer to the manufacturing of freeform optics have been discussed.

The calibration capabilities at the NMI level have been significantly enhanced which will benefit the wider metrological and scientific communities by enabling NMIs and DIs to offer new and enhanced measurement services in asphere and freeform calibration.

A good practice guide was prepared to provide a definition and manufacturing process of reference thermo-invariant standards (aspherical and freeform optical surfaces) made of thermo-invariant materials. These reference standards can be calibrated using ultra-high precision measuring machines (accurate single point or imaging instruments) and the calibration traceability has been carefully established. In this guide, the calibration procedure of innovative reference thermo-invariant asphere as well as freeform optical standards, also called Metrological Reference Surfaces (MRS) is described.

At PTB, the new uncertainty value of the radius measurement for spherical sections has been reported to the quality manager and will be included in the next update of the measurement and calibration capabilities. At LNE, sauftgauges for freeform surface were uploaded onto the website of the project and they can be used for testing min-max fiting algorithms. Further sauftgagues for aspheres and freeforms can be generated for specific uses.

A patent application on “high accuracy radius measurement” was also submitted by PTB, which covers a radius uncertainty of 100 nm for typical (full aperture) spherical sections.

Impact on relevant standards

The consortium was active in International and European metrology activities. Partners participated at the TC-Length annual meetings held at VSL in October 2016 and at VTT-MIKES in October 2017. These partners have participated and presented the progress of the project in the TC-Length annual meeting that held at LNE in October 2018.

Several partners were involved in different standards organisations: ISO TC 172 “Optics and photonics”: DIN NA 027-01-02 "Fachbereich Optik" and ISO TC 213 “Dimensional and geometrical product specifications and verification”. ENS-Cachan actively participated at the French Experts meeting for ISO TC 213 (UNM 08) and at the ISO TC 213 activities (as committee member of WG 18 and WG 12). Furthermore, ENS-Cachan participated at the 42nd international meeting session of ISO/TC 213 and contributed to a new draft for ISO 18183-1: Geometrical product specifications (GPS) - Partitioning - Part1: Overview and Basic concepts. This draft will include the curvature-based approaches for fitting, registration and data fusion that will be developed in the project as the basis of new methods and algorithms for partitioning. LNE also participated in the French ISO TC 213 activities (as committee member of WG 15 and WG 16). PTB participated at the DIN committee NA 027-01 FB "Fachbereich Optik" in June 2017 which contributed to ISO TC 172 SC1.

Longer-term economic, social and environmental impacts

The manufacture of optical surfaces is an iterative process, based on measurements of the current shape of the specimen and subsequent shape correction. The improved measurement capabilities at NMIs/DIs allowed industries to achieve a more accurate measurement of the current shape of optical surfaces. As a direct consequence, the required number of iteration steps can be minimised, leading to a drastically reduced production time and cost per individual asphere and freeform optics.

The outcomes of this project led to improve the reliability, efficiency and speed of asphere and freeform surface production through the improved measurement and traceability capabilities of manufacturers. These improvements avoided waste parts and optimize the number of iteration steps needed for the manufacturing, leading to a reduced environmental impact. By using aspheres and freeform optics which achieve similar or usually better results than multiple large spherical optics, the consumption of material and energy is drastically reduced. Weight and size of optical systems is reduced too. Further improvement of optical components supported the miniaturization of optical systems and helps to protect the environment, saving resources and energy.

6 List of publications

1. P. Křen, Robust and precise algorithm for aspheric surfaces characterization by the conic section, Journal of the European Optical Society. https://doi.org/10.1186/s41476-017-0040-1
2. P. Ekberg, R. Su & R. Leach, High-precision lateral distortion measurement and correction in coherence scanning interferometry using an arbitrary surface, Optics Express. https://doi.org/10.1364/OE.25.018703
3. R. Su, T. Matthew, R. Leach & J. Coupland, Effects of defocus on the transfer function of coherence scanning interferometry, Optics Letters. https://doi.org/10.1364/OL.43.000082
4. Y. Arezki, X. Zhang, C. Mehdi-Souzani, N. Anwer & H. Nouira, Investigation of minimum zone assessment methods for aspheric shapes, Precision Engeneering. https://doi.org/10.1016/j.precisioneng.2018.01.008
5. Y. Arezki, H. Nouira, N. Anwer & C. Mehdi-Souzani, A novel hybrid trust region minimax fitting algorithm for accurate dimensional metrology of aspherical shapes, Measurements. https://doi.org/10.1016/j.measurement.2018.05.071
6. Y.Arezki, C. Mehdi-Souzani, N.Anwer & H.Nouira, Reference data simulation for L_∞ fitting of aspheres, Proceedings of CIRP CAT. https://doi.org/10.1016/j.procir.2018.04.051
7. C. F. Cheung, M. Y. Liu, R. Leach, X. B. Feng & C. Y. Zhao, Hierarchical-information-based characterization of multiscale structured surfaces, CIRP Annals Manufacturing Technology. https://doi.org/10.1016/j.cirp.2018.04.002
8. Speidel, R. Su, J. Mitchell-Smith, P. Dryburgh, I. Bisterov, D. Pieris, W. Li, M. Clark & A. T. Clare, Crystallographic texture can be rapidly determined by electrochemical surface analytics, Acta Materialia https://doi.org/10.1016/j.actamat.2018.07.059
9. Fortmeier, M. Schulz & R. Meeß, Traceability of form measurements of freeform surfaces: metrological reference surfaces, Optical Engineering https://doi.org/10.1117/1.OE.58.9.092602
10. R. Schachtschneider, M. Stavridis, I. Fortmeier, M. Schulz &C. Elster, SimOptDevice: a library for virtual optical experiments, Journal of Sensors and Sensor Systems https://doi.org/10.5194/jsss-8-105-2019
11. X. Feng, N. Senin, R. Su, S. Ramasamy & R. Leach, Optical measurement of surface topographies with transparent coatings, Optics and Lasers in Engineering https://doi.org/10.1016/j.optlaseng.2019.04.018
12. X. Xu, X. Zhang, Z. Niu, W. Wang, Y. Zhu & M. Xu, Self-calibration of in-situ monoscopic deflectometric measurement in precision optical manufacturing, Optics Express https://doi.org/10.1364/OE.27.007523

7 Contact details

Coordinator: Dr. -habil. Hichem Nouira, LNE

Tel: +33 140 433 763
E-mail: hichem.nouira@lne.fr

Project website address: http://www.ptb.de/empir/freeform-home.html